Biomedicine & Pharmacotherapy 192 (2025) 118603

Contents lists available at ScienceDirect

Biomedicine & Pharmacotherapy

journal homepage: www.elsevier.com/locate/biopha

# *N*-Methyl-*N*-((1-methyl-5-(3-(piperidin-1-yl)propoxy)-1*H*-benzo[*d*]imidazol-2-yl)methyl)prop-2-yn-1-amine (MBA-159), a new multitarget small molecule for the therapy of Alzheimer's disease

Óscar M. Bautista-Aguilera [a,*], Aleksandra Manik [b], Daniel Diez-Iriepa [a], Natalia Szałaj [c], Paula Zaręba [c], Anna Więckowska [c], Paweł Żmudzki [d,e], Ewelina Honkisz-Orzechowska [f], Damijan Knez [g], Stanislav Gobec [g], Kinga Sałat [b], Borja Martínez-Alonso [h], Víctor Guarnizo-Herrero [h], Guillermo Torrado Durán [h], Carlos Torrado-Salmerón [i], Aina Bellver-Sanchis [j,k], Inaya Nsiona-Defise [j,k], Marta Ribalta-Vilella [j,k,l], Mercè Pallàs [j,k,m], Francisco López-Muñoz [n,o], Christian Griñán-Ferré [j,k,m,**], José Marco-Contelles [p,***], Isabel Iriepa [a,q,****]

[a] *Universidad de Alcalá, Departamento de Química Orgánica y Química Inorgánica, Instituto de Investigación Química "Andrés M. del Río" (IQAR), Alcalá de Henares, Madrid 28805, Spain*
[b] *Department of Pharmacodynamics, Chair of Pharmacodynamics, Faculty of Pharmacy, Jagiellonian University Medical College, 9 Medyczna St., Krakow 30-688, Poland*
[c] *Department of Physicochemical Drug Analysis, Faculty of Pharmacy Jagiellonian University Medical College, 9 Medyczna St., Krakow 30-688, Poland*
[d] *Department of Medicinal Chemistry, Faculty of Pharmacy, Jagiellonian University Medical College, 9 Medyczna St., Krakow 30-688, Poland*
[e] *Laboratory of Small Molecules, Centre for the Development of Therapies for Civilization and Age-Related Diseases, Jagiellonian University Medical College, 9 Medyczna St., Krakow 30-688, Poland*
[f] *Department of Technology and Biotechnology of Drugs, Faculty of Pharmacy, Jagiellonian University, Medical College, 9 Medyczna St., Krakow 30-688, Poland*
[g] *University of Ljubljana, Faculty of Pharmacy, Askerceva 7, Ljubljana 1000, Slovenia*
[h] *Universidad de Alcalá, Facultad de Farmacia, Departamento de Ciencias Biomédicas, 28805-Alcalá de Henares, Madrid, Spain*
[i] *Universidad Complutense de Madrid, Facultad de Farmacia, Departamento de Farmacia Galénica y Tecnología Alimentaria, Madrid 28040, Spain*
[j] *Pharmacology Section, Department of Pharmacology, Toxicology and Therapeutic Chemistry, Faculty of Pharmacy and Food Sciences, Institute of Neuroscience, Universitat de Barcelona (NeuroUB), Av. Joan XXIII 27–31, Barcelona 08028, Spain*
[k] *Institut de Neurociències, Universitat de Barcelona (NeuroUB), Barcelona, Spain*
[l] *PhD program in Biotechnology, Faculty of Pharmacy and Food Sciences, University of Barcelona, Avda. Joan XXIII 27, Barcelona 08028, Spain*
[m] *Spanish Biomedical Research Center in Neurodegenerative Diseases (CIBERNED)-Instituto de Salud Carlos III, Madrid, Spain*
[n] *Faculty of Health Sciences–HM Hospitals, Camilo José Cela University, Madrid, Spain*
[o] *HM Hospitals Health Research Institute, Neuropsychopharmacology Unit, "Hospital 12 de Octubre" Research Institute, Madrid, Spain*
[p] *Institute of General Organic Chemistry (CSIC), C/ Juan de la Cierva 3, Madrid 28006, Spain*
[q] *Grupo DISCOBAC, Instituto de Investigación Sanitaria de Castilla-La Mancha (IDISCAM), Spain*

ARTICLE INFO

*Keywords:*
ADME
Alzheimer's disease
Biological evaluation
Molecular modelling

ABSTRACT

As part of a project aimed at the pharmacological optimization of Contilisant, herein we describe molecular modelling studies that led to the identification of **MBA-159** as a new polyfunctionalized, multitarget-directed ligand and a promising drug candidate for the treatment of Alzheimer's disease. We synthesized **MBA-159** and conducted comprehensive *in vitro* and *in vivo* evaluations. In *in vivo* studies **MBA-159** demonstrated favourable pharmacokinetics, anti-amnesic properties and significantly improved non-spatial memory (contextual and recognition memory) in a mouse model of scopolamine-induced amnesia. Additionally, **MBA-159**

* Corresponding author.
** Corresponding author at: Pharmacology Section, Department of Pharmacology, Toxicology and Therapeutic Chemistry, Faculty of Pharmacy and Food Sciences, Institute of Neuroscience, Universitat de Barcelona (NeuroUB), Av. Joan XXIII 27–31, Barcelona 08028, Spain.
*** Correspondence to: Laboratory of Medicinal Chemistry, Institute of General Organic Chemistry (CSIC), C/ Juan de la Cierva, 3, Madrid 28006, Spain.
**** Corresponding author at: Universidad de Alcalá, Departamento de Química Orgánica y Química Inorgánica, Instituto de Investigación Química, "Andrés M. del Río" (IQAR), Alcalá de Henares, Madrid 28805, Spain.
*E-mail addresses:* oscar.bautista@uah.es (Ó.M. Bautista-Aguilera), iqoc21@iqog.csic.es (J. Marco-Contelles), isabel.iriepa@uah.es (I. Iriepa).

https://doi.org/10.1016/j.biopha.2025.118603

Available online 27 September 2025

Pharmacokinetic analysis
Synthesis

showed a tendency to increase synaptic plasticity biomarkers and reduce neuroinflammatory trends (assessed by qPCR), as well as cognitive enhancement in a senescence-accelerated prone mouse 8 model.

## 1. Introduction

Alzheimer's disease (AD) is a neurodegenerative disorder characterized by progressive memory decline, a process that involves a variety of cognitive domains, including attention, language comprehension, and problem-solving skills [1], whose deficits contribute to a poor level of social interaction and decreased quality of life [2]. AD is the most commonly diagnosed form of dementia with a significant impact on public health. According to the current data, more than 55 million people are living with dementia, and this number will almost triple by 2050 as a result of ageing [3]. As research has progressed, a number of mechanisms have been proposed to explain the etiology of AD, including the abnormal aggregation of certain proteins in the central nervous system (CNS), such as amyloid-$\beta$ (A$\beta$) peptide, and tau protein [4], familial genetic mutations [5], and brain lesions caused by environmental factors [6]. However, despite extensive efforts, the precise origins and causes of AD remain unclear.

Consequently, and unsurprisingly, there are only a few drugs available for the treatment of AD. While several procognitive acetyl- and/or butyrylcholinesterase inhibitors (AChEIs/BuChEIs), such as tacrine, galantamine, donepezil, and rivastigmine, are approved for mild-to-moderate AD by enhancing ACh levels, and memantine, a *N*-methyl-D-aspartate (NMDA) receptor antagonist, is used for moderate-to-severe AD, their long-term clinical use suggests they only provide temporary cognitive improvement. These treatments fail to prevent neuronal loss, halt dementia progression or modify the course of the disease [7]. Additionally, many patients experience serious side effects, including CNS disorders, gastrointestinal disturbances or cardiac arrhythmias, or hepatotoxicity, as in the case of tacrine, a fact that determined its withdrawal from the clinic [8]. In a pursuit of disease-modifying treatment, monoclonal antibodies targeting amyloid-beta plaques were developed and approved by the FDA in 2021 (aducanumab), 2023 (lecanemab) and in 2024 (donanemab). However, aducanumab has already been withdrawn from the market. While promising, their effects remain limited, highlighting the urgent need for the development of new and more effective therapeutic alternatives for the treatment of AD [9].

At the beginning of the 21st century, a new strategy "*one molecule-multiple targets*" was proposed in medicinal chemistry for the development of ligands to treat multifactorial diseases [10]. We have proposed to call them Multitarget Small Molecules (MSMs) [11]. For AD, many potential combinations have been reported, mostly combining AChEIs with other biological targets, e.g. monoamine oxidase A/B (MAO A/B) inhibition, antioxidant or neuroprotective properties [11]. Several years ago, we conceptualized for the first time the combination of histamine 3 receptor (H3R)/ sigma-1 receptor (S1R) modulation with AChE/BuChE, and MAO A/B inhibition an MSM [12]. This project was then further developed and led to the identification of **Contilisant (1)** (Fig. 1 [13]), which was developed based on the structure of previously described MSM **ASS234 (2)** (Fig. 1) [14], which carries a propargyl group known to be responsible MAO inhibition (Fig. 1) [15]. **Contilisant** was the first described permeable, neuroprotective and antioxidant MSM with high affinity for human H3R (*h*H3R, $Ki$ = 10.8 nM) and S1R ($Ki$ = 65 nM), which inhibited hMAO B ($IC_{50}$ = 78 nM) and hAChE ($IC_{50}$ of 530 nM) [12,13]. At a dose of 1 mg/kg i.p., **Contilisant** was able to restore lipopolysaccharide-induced memory deficit in the novel recognition test in mice [12], and significantly attenuate the cognitive deficit induced by A$\beta_{1-42}$ in the radial maze assay in an *in vivo* learning and memory task, comparing very favourably with donepezil (Aricept®) [13]. Recently, in a project targeted to the pharmacological optimization of **Contilisant,** we reported the synthesis and biological evaluation of **Contilisant**+**Tubastatin A** hybrids and identified **MTP-100 (3)** and **MTP-109 (4)** (Fig. 1) as MSMs that, in addition, inhibit histone deacetylases 1,6 [16].

Based on these results, we have launched a new project aimed at improving the pharmacological profile of **Contilisant**, which resulted in a new MSM **MBA-159** (Fig. 1). Molecular modelling was first employed to select the new ligand, followed by its synthesis and *in vitro* and *in vivo* biological evaluation, which has confirmed that **MBA-159** is a new MSM possessing anti-amnesic properties, significantly improving non-spatial memory (contextual and recognition memory) in a mouse model of scopolamine-induced amnesia, showing also tendency to increase *Forkhead box protein p2* (*Foxp2*) and *Cathecol-O-methyltransferase* (*Comt*) expression in a senescence-accelerated prone mouse 8 model (SAMP8).

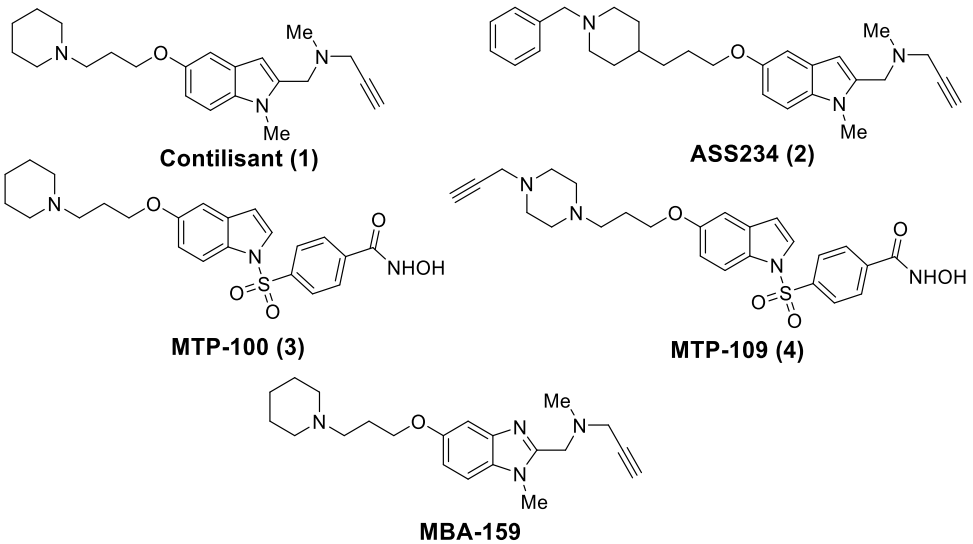


**Fig. 1.** Structures of **Contilisant** (1), **ASS234** (2), **MTP-100** (3), **MTP-109** (4), and **MBA-159**.

## 2. Results and discussion

### 2.1. Molecular modelling studies

*In silico* drug design methods, using computational techniques, are a powerful tool for reducing the number of ligands that need to be synthesized and screened in experimental assays [17], accelerating hit identification and hit-to-lead optimization process, as molecular docking is one of the most widely used methods for the design of multitarget drugs [18]. In this work, docking studies were performed for some analogues of **Contilisant** (**1**) (Fig. 2) in multiple targets related to AD pathogenesis to explore the binding modes of these compounds and to find novel H3R antagonists, S1R agonists, as well as AChEIs, BuChEIs and MAO A/B inhibitors (MAOIs), that can be effective in the treatment of AD.

*In silico* molecular docking studies using AutoDock Vina [19] were performed to explore the affinity and binding interactions of compounds **5**–**7** (Fig. 2) in the binding site of the target proteins and receptors (see Supporting Information). Compounds **5**–**7** (Fig. 2) result from the incorporation of a second heteroatom such as "*O*" to give a C5 substituted benzoxazole (**5**), "*S*" to give a C5 substituted benzothiazole (**6**), and "*N*" to give a C5 substituted benzimidazole (**7**), that perfectly mimic the functional groups and structure in **Contilisant** (**1**) (Fig. 2).

Based on the computational analysis (see Supporting Information), and in spite that the docking scores for compounds **5**–**7** are very similar, the selection of compound **7** was based on an integrated analysis that also considered qualitative differences in binding interactions (hydrogen bonding, hydrophobic contacts, π–π stacking) as well as pharmacokinetic and drug-likeness profiles. Thus, ligand **7**, renamed as **MBA-159**, showed acceptable binding affinities on the selected biological targets. Consequently, we decided to analyze its ADME, synthesize it, and to analyze its pharmacological properties. The selection of benzimidazole **7** is not surprising, as this scaffold has been efficiently applied in the design of original drug candidates for the treatment of AD [20].

### 2.2. In silico ADME analysis of MBA-159

Theoretical calculations of the ADME (Absorption, Distribution, Metabolism and Excretion) properties of compound **MBA-159** were done to assess its druggability. Numerous physically significant descriptors and pharmacologically relevant properties were predicted and analyzed (Table S1, Supporting Information). The results suggest that compound **MBA-159** does not violate Lipinski's rules [21] (ROF) and the Qikprop's rule of three [22,23] (ROT). Almost all calculated descriptors and properties are within the expected Qikprop thresholds except the estimated number of hydrogen bond donors (donorHB) and acceptors (accptHB). Aqueous solubility (QPlogS) of organic molecules plays a key impact on many ADME-related properties. Compound **MBA-159** showed solubility values within the limits (QPlogS = −3.361; limits −6.5–0.5). The partition coefficient (QPlogPo/w), critical for the estimation of absorption within the body, is in the recommended range (QPlogPo/w = 3.747; limits −2.0–6.5) (Table S1). It was also predicted to be active against the central nervous system (CNS = 2). Among all the properties, the predicted value for the Blood Brain Barrier (BBB) penetration (QPlogBB: acceptable range −3.0–1.2) is a very important parameter, indicating the ability of the molecule to pass through the blood-brain barrier, which is mandatory for AD treatment. The predicted logBB values for compound **MBA-159** (QPlog BB = 0.614 see Table S1, Supporting Information) are in the optimum range. Polar Surface Area (PSA) is a measure of a molecule's hydrogen bonding capacity, and its value should not exceed a certain limit if the compound is intended to be CNS active. Molecules with PSA < 100 Å$^2$ are more likely to penetrate the BBB and the most active CNS drugs have PSA lower than 70 Å$^2$. The value of PSA for compound **MBA-159** is 31.938 A$^2$ and it is within the range. The percentage of human oral absorption for the compound is very high (95.681 %) (see Table S1, Supporting Information). Other physicochemical descriptors obtained by QikProp (Table S1, Supporting Information) are within the acceptable range for human use.

In conclusion, this study reveals that the designed compound **MBA-159** has appropriate pharmacokinetic properties as a suitable and possible CNS drug. Consequently, next, we prepared multigram amounts to test it in different experimental *in vitro* and *in vivo* assays.

### 2.3. Synthesis of MBA-159

The synthesis of the molecule **MBA-159** has been carried out as shown in Scheme 1 in six steps, starting from commercially available 4-methoxy-2-nitroaniline (**8**). Monoalkylation of aniline **8** with methyl

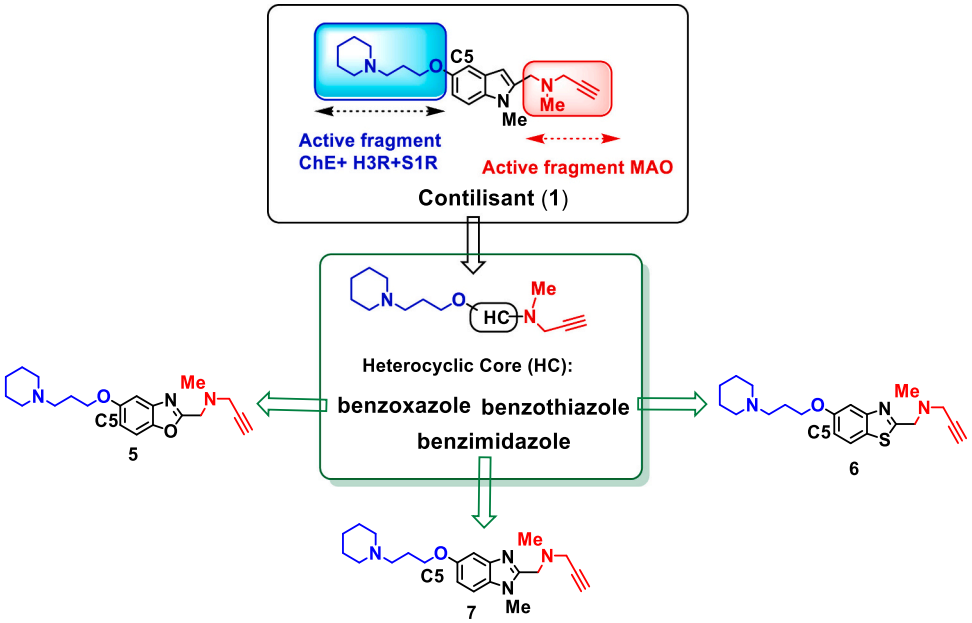


**Fig. 2.** Chemical structures of **Contilisant** and the proposed, *in silico* investigated structures 5–7.

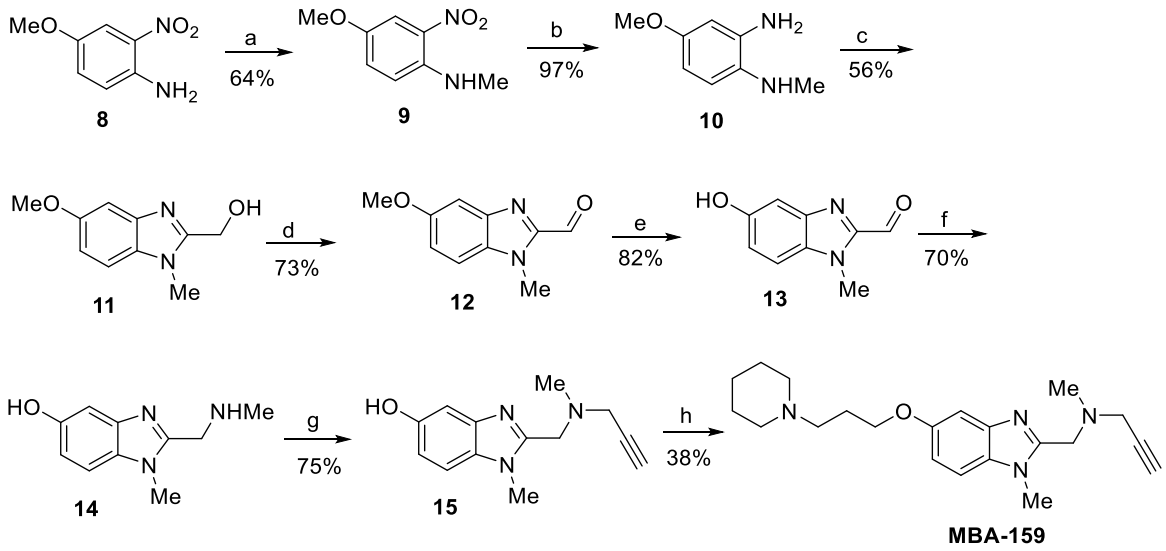


**Scheme 1.** Reagents and conditions: (a) NaH, DMF, MeI, 0 ºC; (b) $H_2$, Pd/C 5 %, EtOAc/EtOH, 40 ºC; (c) aq. HCl (5.0 M), glycolic acid, 100 ºC; (d) Dess–Martin periodinane, DCM, 0 ºC; (e) $BBr_3$, DCM, - 75 ºC; (f) i. $NH_2Me$ (2.0 M) in MeOH, $Na_2SO_4$, rt ii. $NaBH_4$, rt; (g) Propargyl bromide, DIPEA, THF, 0 ºC; (h) NaH, DMF, 1-(3-chloropropyl)piperidine hydrochloride, rt.

iodide, in the presence of NaH in DMF, gave 4-methoxy-*N*-methyl-2-nitroaniline (**9**) [24], which was reduced to afford 4-methoxy-$N^1$-methylbenzene-1,2-diamine (**10**) [25]. In the next step, the imidazobenzene moiety was installed by reacting diamine **10** with glycolic acid in HCl medium to give (5-methoxy-1-methyl-1*H*-benzo[*d*]imidazol-2-yl)methanol (**11**) [26], which was oxidized using Dess-Martin periodinane to afford 5-methoxy-1-methyl-1*H*-benzo[*d*]imidazole-2--carbaldehyde (**12**) [27]. Following *O*-demethylation with boron tribromide furnished 5-hydroxy-1-methyl-1*H*-benzo[*d*]imidazole-2-carbal dehyde (**13**), which was subjected to reductive alkylation with methylamine and sodium borohydride to furnish amine **14**, which was *N*-alkylated with propargyl bromide to yield **15**, followed by *O*-alkylation with commercial 1-(3-chloropropyl)piperidine hydrochloride, in the presence of NaH, DMF, to obtain the target *N*-methyl--*N*-((1-methyl-5-(3-(piperidin-1-yl)propoxy)-1*H*-benzo[*d*]imidazol-2-yl) methyl)prop-2-yn-1-amine (**MBA159**). All new compounds gave spectroscopic and analytical data in good agreement with their structures (**Experimental Part**, Supporting Information). With compound **MBA-159** in our hands, next, we started its biological evaluation.

## 2.4. *In vitro experiments*

### 2.4.1. *Solubility and metabolic stability*

For **MBA-159** and **Contilisant**, we assessed metabolic stability and thermodynamic solubility (Table 1). Metabolic stability in mouse liver microsomes (MLM) was evaluated in the presence of NADPH, primarily to examine CYP450-dependent metabolism, with verapamil used as a positive control. To address potential challenges associated with poor solubility, such as variable and limited intestinal absorption, we conducted thermodynamic solubility studies. This *in vitro* evaluation highlighted a clear advantage of MBA-159, particularly due to its five-fold higher thermodynamic solubility, while both compounds demonstrated high metabolic stability compared to verapamil.

**Table 1**
Metabolic stability and solubility data for compound MBA-159.

| Compd. | MLM stability (%)[a] ± SD | Solubility (mg/mL)[b] ± SD |
|---|---|---|
| **MBA−159** | 94 ± 2 | 1.4 ± 0.0 |
| **Contilisant** | 97 ± 1 | 0.3 ± 0.1 |

[a]Value is the percentage remaining of 1 μM **MBA-159 and Contilisant** after 15 min incubation with mouse liver microsomes (MLM). Verapamil was used as a positive control (35 % compound remaining after 15 min). [b]Concentration of **MBA-159 and Contilisant** in Dulbecco's phosphate-buffered saline (DPBS) after 24 h shaking at room temperature. Values are means of at least two experiments.

### 2.4.2. *Neurotoxicity and hepatotoxicity*

The fundamental functioning of the CNS is based on transmitting and processing signals in the brain. The new drug targeting the CNS must not hinder this process. For that reason, the issue of neurotoxicity is essential. On the other hand, the liver safety of new compounds that are developed as early as the preclinical development phase is important since the liver is a central player in the metabolism of most drugs. To eliminate this risk of drug-induced hepatotoxicity, the effect of **MBA-159** on the human hepatocellular carcinoma cells HepG2 (ATCC® no. HB8065™) was evaluated with the MTS assay. Neurotoxicity and hepatotoxicity were evaluated by treating SH-SY5Y and HepG2 cells, respectively, with compound **MBA-159** in a wide range of concentrations (0.75–100 μM) (Figs. 3 and 4). In both cellular models, **MBA-159** showed an excellent safety profile and did not affect cell viability. Examination under an inverted microscope did not reveal any precipitation of the compound in the culture medium. In comparison, doxorubicin in the same concentration range exerted a significant cytotoxic effect on both cell lines. Although the anti-tumor drug doxorubicin is not a typical CNS-acting drug, its selection as a reference compound in this study was based on recent results published by Imosemi and colleagues [28] who showed that doxorubicin was neurotoxic in rats and it significantly influenced the activity of acetylcholinesterase, a key enzyme involved in the cholinergic neurotransmission and the molecular target for memory-improving drugs. Similar results were obtained by Okudan and colleagues [29].

### 2.4.3. *In vitro biological evaluation of MBA-159*

The inhibitory activities of **MBA-159** and **Contilisant** (**1**) on MAO A/B were determined by Amplex Red-HRP coupled assay and for the ChEs using Ellman's method [30]. As shown in Table 2, **MBA-159** is a very modest hMAO-AI, while the hMAO-B inhibition could not be determined due to poor dose response. **MBA-159** is also a selective, yet not potent hAChEI. 2,2-Diphenyl-1-picrylhydrazyl (DPPH) assay was used to determine the capacity of compounds to reduce DPPH radicals. Results are expressed as DPPH reduction [%] in comparison to resveratrol and Trolox, which were used as a positive control (Resveratrol: 87 % DPPH reduced; Trolox: 97 % DPPH reduced; Resveratrol: $EC_{50}$ = 50.1 ± 4.6 μM). As shown in Table 2, **MBA-159** is a very modest antioxidant

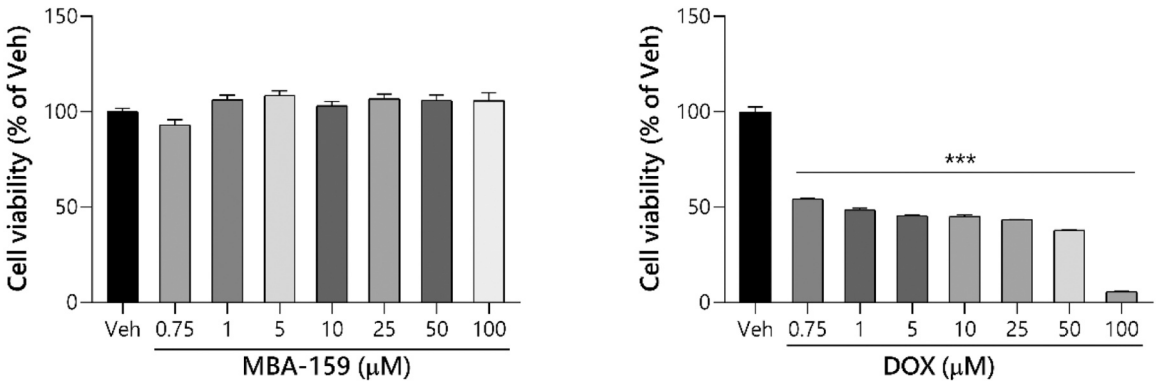


**Fig. 3.** The cytotoxicity of **MBA-159** and doxorubicin (DOX) on HepG2 cells after 72 h. Each point represents the mean ± SEM of three independent experiments, each of which consisted of four replicates per treatment group (n = 12). Statistical analyses were performed using GraphPad Prism 8.0 software. Statistical significance was evaluated by one-way ANOVA with *post hoc* Dunnett's test at significance level α = 0.05 (*** $p < 0.001$).

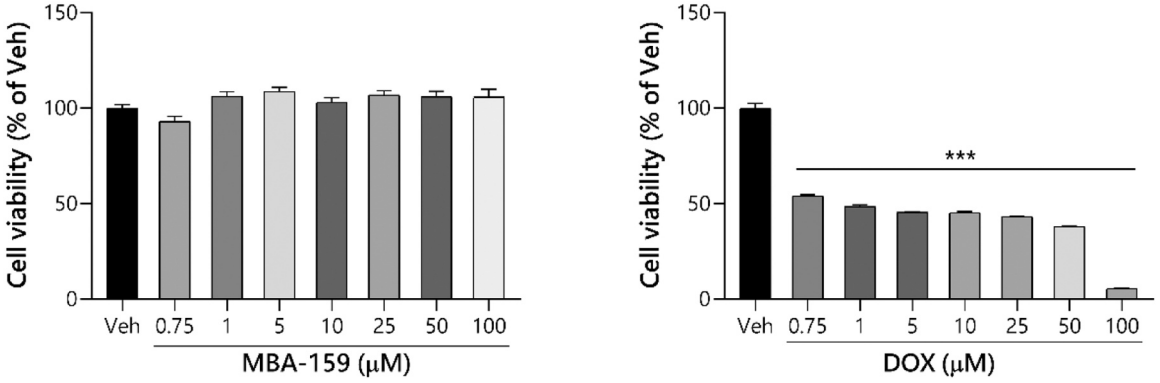


**Fig. 4.** The cytotoxicity of **MBA-159** and doxorubicin (DOX) on SH-SY5Y cells after 72 h. Each point represents the mean ± SEM of three independent experiments, each of which consisted of four replicates per treatment group (n = 12). Statistical analyses were performed using GraphPad Prism 8.0 software. Statistical significance was evaluated by one-way ANOVA with *post hoc* Dunnett's test at significance level α = 0.05 (*** $p < 0.001$).

**Table 2**
$IC_{50}$ values (μM) for the inhibition of hMAOs and hChEs by **MBA-159** and **Contilisant**, and their DPPH scavenging activity ($EC_{50}$, μM).

| Compound | hMAO-A | hMAO-B | hAChE | hBuChE | DPPH scavenging [% of DPPH reduced] |
|---|---|---|---|---|---|
| **MBA−159** | 28.8 ± 5.7 | n.d.[a] | 53.8 ± 0.9 | n.a.[b] | 2041 ± 58 μM |
| **Contilisant** | 0.356 ± 0.027 | 1.56 ± 0.11 | n.a.[b] | 90.7 ± 16.6 | 1519 ± 49 μM |

$IC_{50}$ values are expressed as mean ± SEM (n = 3); [a] n.d., not determined (no clear dose-response, residual activity – RA at 100 μM = 39 %, at 100 μM = 77 %); [b]n.a., not active (RA at 100 μM >50 %).

with comparable radical-scavenging activity to **Contilisant**. Finally, the capacity of compounds to inhibit $A\beta_{1-42}$ aggregation was assessed in the Thioflavin T assay as described previously [31]. Compound **MBA-159** does not influence the aggregation of $A\beta_{1-42}$ under the assay conditions used.

### 2.5. *In vivo biological evaluation experiments*

#### 2.5.1. *In vivo pharmacokinetic experiments*

*2.5.1.1. MBA-159 and Contilisant HPLC-MS/MS Assay: Determination of content in plasma.* An HPLC-MS/MS assay was developed and validated to quantify **MBA-159** and **Contilisant** in plasma. A modular Agilent 1100 series (Agilent, Waldbroon, Germany) equipped with a quaternary pump was used. Each compound was separated using a column KINETEX F5 (2,6 μm × 2,1 mm × 100 mm), and the temperature of column was maintained at 36 °C.

For the separation of **MBA-159** a binary gradient containing water in mobile phase A (0.1 % formic acid) and acetonitrile (0.1 % formic acid) in mobile phase B was used with a flow rate of 0.3 mL/minute and an injection volume of 5 μL (detailed in Table 3).

For the separation of **Contilisant** it was used and inverse binary gradient in comparison with **MBA-159**, also containing water in mobile phase A (0.1 % formic acid) and acetonitrile (0.1 % formic acid) in mobile phase B was used with a flow rate of 0.3 mL/minute and an injection volume of 5 μL (detailed in Table 4).

The MS-MS detection was carried out using a Thermo TSQ Quantum LC/MS Triple Quadruple instrument (Waltham, MA, USA) equipped with electrospray (ESI) source in the positive mode, and detection was performed in a multiple reaction monitoring (MRM) mode. Optimization of the fragments and collision energies of the protonated precursor ion was made, and the following results were obtained and included in the acquisition method (Table 5).

*2.5.1.2. Pharmacokinetic study.* **Contilisant** has been shown to be a safe drug for the treatment of neurodegenerative diseases, however, there are limited pharmacokinetic studies characterising its behaviour [32]. In this section, pharmacokinetic studies of two formulations of suspensions of carboxymethyl cellulose at 0.35 % (w/w) with **Contilisant** or **MBA-159** were administered to two groups of rats. Doses equivalent to 30 mg/kg for each active ingredient were administered. Plasma

**Table 3**
Binary gradient mobile phase HPLC-MS/MS for **MBA-159**.

| Time (min) | Flow rate (mL/ min) | Mobile phase A (%) | Mobile phase B (%) |
|---|---|---|---|
| 0.0 | 0.300 | 80.0 | 20.0 |
| 3.0 | 0.300 | 80.0 | 20.0 |
| 4.0 | 0.300 | 20.0 | 80.0 |
| 7.0 | 0.300 | 20.0 | 80.0 |
| 8.0 | 0.300 | 80.0 | 20.0 |
| 19.0 | 0.300 | 80.0 | 20.0 |
| 20.0 | 0.300 | 80.0 | 20.0 |

**Table 4**
Binary gradient mobile phase HPLC-MS/MS for **Contilisant**.

| Time (min) | Flow rate (mL/ min) | Mobile phase A (%) | Mobile phase B (%) |
|---|---|---|---|
| 0.0 | 0.300 | 20.0 | 80.0 |
| 3.0 | 0.300 | 20.0 | 80.0 |
| 4.0 | 0.300 | 80.0 | 20.0 |
| 7.0 | 0.300 | 80.0 | 20.0 |
| 8.0 | 0.300 | 20.0 | 80.0 |
| 19.0 | 0.300 | 20.0 | 80.0 |
| 20.0 | 0.300 | 20.0 | 80.0 |

concentrations of **Contilisant** and **MBA-159** were analyzed by HPLC-MS/MS, as shown in Fig. 5.

In this pharmacokinetic study, a direct relationship was observed between the hydrophilic/lipophilic ratio of the **Contilisant** and **MBA-159** and their pharmacokinetic profiles. Specifically, **Contilisant**, which exhibits a relatively higher hydrophilicity, reached a rapid maximum concentration (Cmax) at 0.5 h, while **MBA-159**, with a more pronounced lipophilic character, showed a significant increase in Cmax at 1 h (Fig. 5). Several studies have indicated that the enhanced absorption of lipophilic drugs is attributable to their improved ability to cross transcellular barriers [33]. Additionally, Fig. 5 shows a second concentration peak for both compounds at 5 h, a phenomenon typically associated with the enterohepatic recirculation of drug formulations [34].

The mean pharmacokinetic parameters (Cmax, Tmax and AUC0–24 h) are summarized in Table 6. The data revealed significant improvements in the Cmax, rate and extent of drug absorption of **MBA-159** compared to **Contilisant**. Previous studies with different lipophilic systems showed increased plasma concentrations, which could be related to an increase in absorption attributed to different mechanisms: transcellular or lymphatic absorption [33].

The relative bioavailability of **MBA-159** was about 387.36 % compared to **Contilisant**, indicating faster absorption and higher bioavailability. Furthermore, the mean Cmax of **MBA-159** showed a substantial increase ($p < 0.001$) of 69.96 % compared to **Contilisant**. However, other pharmacokinetic parameters such as elimination rate constant ($K_e$) and half-life ($t_{½}$) did not differ significantly between both formulations. These pronounced differences in bioavailability could be attributed to the enhanced intestinal membrane permeability of **MBA-159.** Further studies, including BBB permeability and concentration in the brain, will be important to evaluate the potential of **MBA-159** in the treatment of neurodegenerative diseases.

**Table 5**
Optimized mass spectrometry parameters.

| Compound | Precursor ion (*m/z*) | Quantification ion (*m/z*) | Collision energy (V) |
|---|---|---|---|
| **MBA−159** | 355.334 | 98.327 | 33 |
| | 355.334 | 126.302 | 32 |
| | 355.334 | 286.307 | 21 |
| **Contilisant** | 354.325 | 98.318 | 33 |
| | 354.325 | 126.299 | 32 |
| | 354.325 | 200.178 | 21 |

Capillary temperature 300 ºC; sheath gas pressure 40 L/h; capillary voltage, 3 kV.

*2.5.2. The effect of the test compound MBA-159 on learning and memory in mice*

Cognitive impairments and memory decline might result from several factors, including advanced age, neurodegenerative disorders, and chronic stress. Currently available drugs used to attenuate dementia are weakly effective and they are able to improve learning and memory skills only in the early phase of the disease. Therefore, novel antiamnesic drugs and drug candidates are strongly needed. Considering this, the aim of this *in vivo* research was to assess the ability of the compound **MBA-159** to attenuate learning and memory deficits resulting from the dysfunction of the cholinergic system. A nonselective muscarinic receptor antagonist, namely scopolamine, was used to induce amnesia and cognitive decline resembling that observed in the course of AD [35]. Two complementary behavioural assays were used to assess the effect of the test compound on learning and memory in mice, namely the passive avoidance (PA) task and the novel object recognition (NOR) task. Also, as a part of the safety pharmacology study, locomotor activity and rotarod tests were used to assess the effect of **MBA-159** on animals' motor coordination.

*2.5.2.1. Passive avoidance task.* In this fear-motivated task, the effect of three doses of **MBA-159** (5, 10 and 30 mg/kg) on scopolamine-induced cognitive dysfunction was assessed. A significant overall effect of treatment was observed ($F_{[4,90]} = 5.531$, $p < 0.001$). Time effect and drug x time interaction were also significant ($F_{[1,90]} = 20.98$, $p < 0.0001$, and $F_{[4,90]} = 7.847$, $p < 0.0001$, respectively). In the acquisition trial, statistically significant inter-group differences in the step-through latency between vehicle-treated mice and scopolamine-treated control group, as well as between scopolamine-treated control mice and **MBA-159-**treated memory-impaired mice were not observed (Fig. 6). In contrast to this, statistically significant differences were observed in the retention trial between scopolamine-treated control and vehicle-treated mice not treated with scopolamine ($p < 0.0001$), as well as between scopolamine-treated control mice and mice that received combined scopolamine and **MBA-159** at doses 5 and 10 mg/kg ($p < 0.05$). The dose 30 mg/kg of **MBA-159** was not effective in this assay (Fig. 6).

These *in vivo* data obtained in the PA task suggest a lack of clear dose-dependency for **MBA-159**. Several reasons may explain this observation, including pharmacokinetic properties of this compound, i.e., its limited CNS exposure, or saturation effects noted for **MBA-159** used at higher dose regimens. Also, the loss of biological activity observed for the highest tested dose of the test compound (30 mg/kg) may be due to the potential involvement of additional molecular targets for modulating the activity of the tested compound administered to mice at a higher concentration. The effect of **MBA-159** on additional molecular targets may not be apparent in the dose range up to 10 mg/kg, but may be noticed for the dose of 30 mg/kg and it may reduce the beneficial pro-cognitive effect of the test compound used at lower doses. Other potential factors responsible for the observed lack of clear dose-dependency observed in the PA task may comprise **MBA-159-**induced toxicity, or receptor desensitization if this compound was used at 30 mg/kg. At this moment, these are only our speculations - the issue requires further extended studies.

*2.5.2.2. Novel object recognition task.* In the NOR task, the discrimination index (DI) was calculated. This parameter reflected the preference of mice to explore a novel (C) or a familiar (A) object in the T2 trial; the higher DI value indicated a stronger preference for the novel (C) object. A significant overall effect of treatment was observed in the NOR test ($F_{[4,34]} = 16.99$, $p < 0.0001$). The comparison of the two control groups

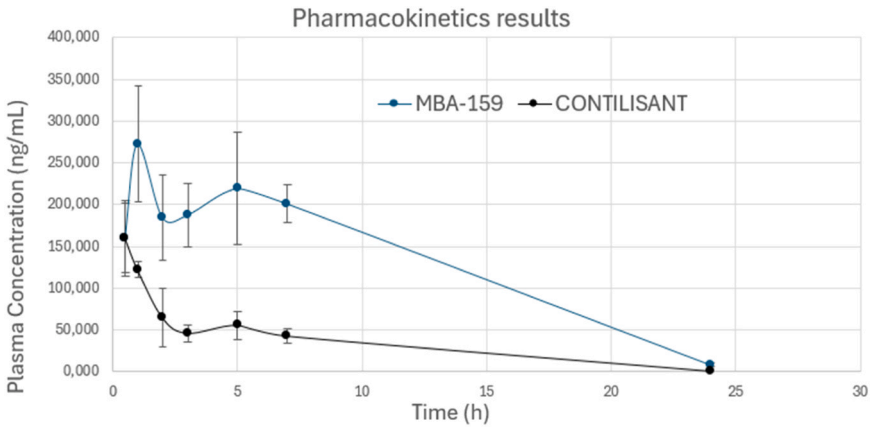


**Fig. 5.** Plasma concentration profile of **MBA-159** (blue) and Contilisant (black) suspension formulations. Mean ± SD for n = 6 (Dose of 30 mg/kg).

**Table 6**
Pharmacokinetic parameters of **MBA-159** and **Contilisant**.

| Parameters | MBA-159 | Contilisant |
|---|---|---|
| $C_{max}$ (ng/mL) | 272.49 ± 11.86 | 160.33 ± 9.23 |
| $T_{max}$ (h) | 1 | 0.5 |
| $C_{24\ h}$ (ng/mL) | 8.39 ± 0.22 | 2.33 ± 0.57 |
| $AUC_{0\text{-}24h}$ (ng h/mL) | 3170.48 ± 157.90 | 818.48 ± 35.81 |
| Ke ($h^{-1}$) | 0.18 | 0.14 |
| $t_{½}$ (h) | 3.90 | 5.10 |

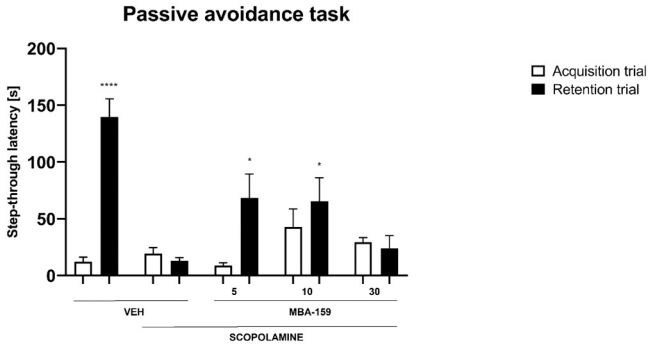


**Fig. 6.** Effect of **MBA-159** (doses: 5, 10 and 30 mg/kg, i.p.) on fear-motivated contextual learning and memory measured using the passive avoidance task in a mouse model of scopolamine-induced amnesia. Results are shown as mean step-through latency (± SEM) assessed in the acquisition trial and 24 h later (in the retention trial) for n = 9–12 mice. Statistical analysis: repeated measures ANOVA followed by Dunnett's *post hoc* comparison. Significance *vs.* scopolamine-treated control mice in the retention trial: * $p < 0.05$ and **** $p < 0.0001$.

(i.e., control not treated with scopolamine *vs.* scopolamine-exposed control) demonstrated that scopolamine (1 mg/kg) induced memory deficits in mice, and it significantly decreased the DI ($p < 0.0001$, Fig. 7). In contrast to this, the mice treated with scopolamine and **MBA-159** at doses 5, 10 and 30 mg/kg exhibited statistically significant ($p < 0.01$) preference for the novel (C) object during the recognition (T2) phase. This effect was similar to that obtained previously for tacrine which was effective in the NOR task at the same dose range (data unpublished).

The difference in the results obtained for **MBA-159** in the PA task (active at doses 5 and 10 mg/kg) and in the NOR task (active at 5, 10 and 30 mg/kg) can be easily explained as these two tasks are complementary to each other and they assess distinct types of memory (contextual, fear-motivated memory – PA task *vs.* visual memory – NOR task).

As shown in our previous paper [30] rivastigmine, the FDA-approved

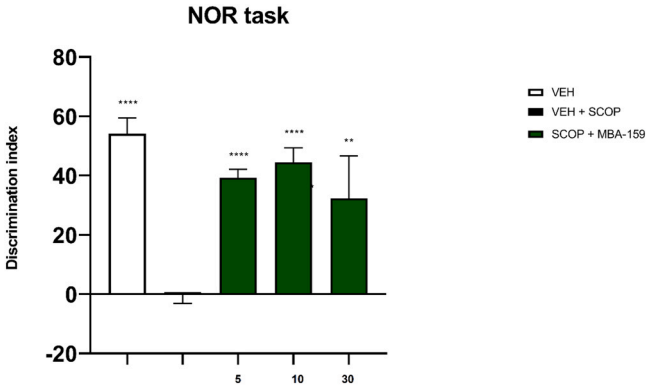


**Fig. 7.** Effects of **MBA-159** (doses: 5, 10, 30 mg/kg, i.p.) on scopolamine-induced memory deficits assessed in the mouse NOR task. Scopolamine was administered s.c. 30 min before the T1 trial and MBA-159 was administered i.p. 60 min before the T1 trial. Data represent mean ± SEM for n = 8–9. Statistical analysis: one-way ANOVA followed by Dunnett's *post hoc* comparison. Significance *vs.* scopolamine-treated control: ** $p < 0.01$, **** $p < 0.0001$.

drug for AD, was highly effective in the PA and NOR tasks at doses 1 and 2.5 mg/kg, but at these doses it induced severe and dose-dependent motor impairments in mice. Such adverse effects were not observed for **MBA-159** (see below).

Since the dose of 10 mg/kg of **MBA-159** was the highest dose effective in both PA and NOR tasks, it was also assessed for its potential ability to induce motor deficits in mice. For this purpose, the rotarod test and the locomotor activity test were carried out.

*2.5.2.3. Rotarod test.* In the rotarod test the effect of intraperitoneally administered **MBA-159** (10 mg/kg) on motor skills in mice was assessed using the rotarod apparatus revolving at 6, 18 and 24 rpm. In this assay, statistically significant motor deficits in mice treated with **MBA-159** were observed only at 24 rpm ($p < 0.05$, Fig. 8C).

*2.5.2.4. Locomotor activity test.* The effect of **MBA-159** used at a dose of 10 mg/kg on animals' locomotor activity was measured using actimeters. The results obtained during the 30-minute test showed no statistically significant differences between the **MBA-159**-treated group and the control group (Fig. 9).

To sum up, the results of the present *in vivo* study revealed statistically significant antiamnesic properties of the compound **MBA-159** in a mouse model of scopolamine-induced amnesia. This antiamnesic activity was observed only for selected doses of **MBA-159** in the PA task and for all doses tested in the NOR task. In order to induce amnesia

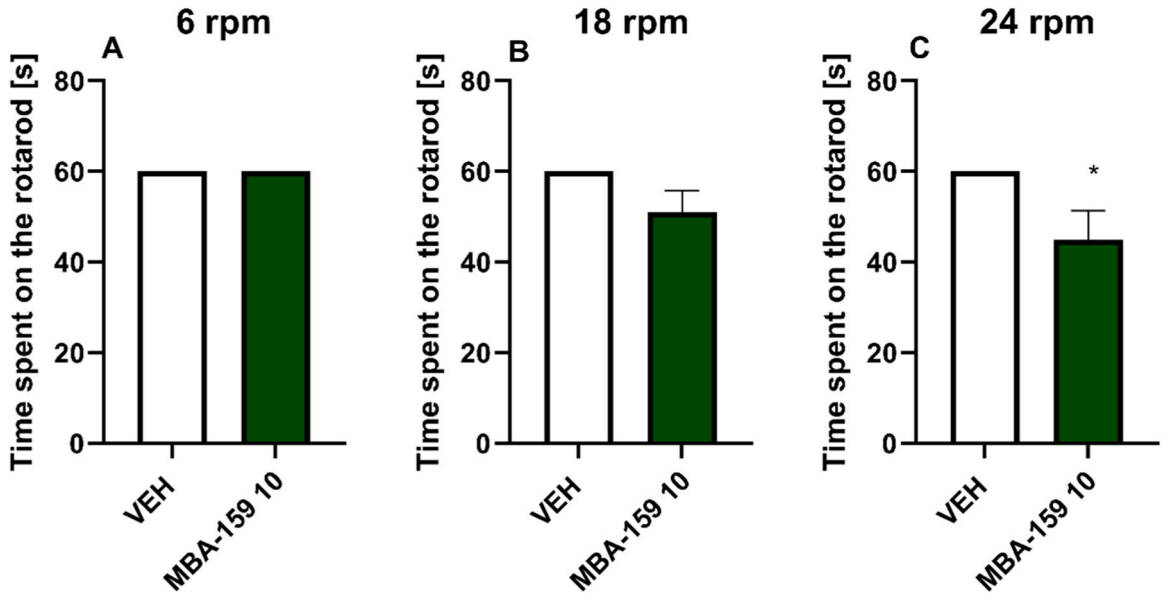


**Fig. 8.** Effect of **MBA-159** (10 mg/kg, i.p.) on motor coordination measured using the rotarod test at 6 rpm (A), 18 rpm (B) and 24 rpm (C). Results for n = 10 are shown as the mean time spent on the rotarod apparatus ± SEM and measured during the 1-min (for each speed) test. Statistical analysis: Student's *t*-test. Significance *vs.* control: * $p < 0.05$.

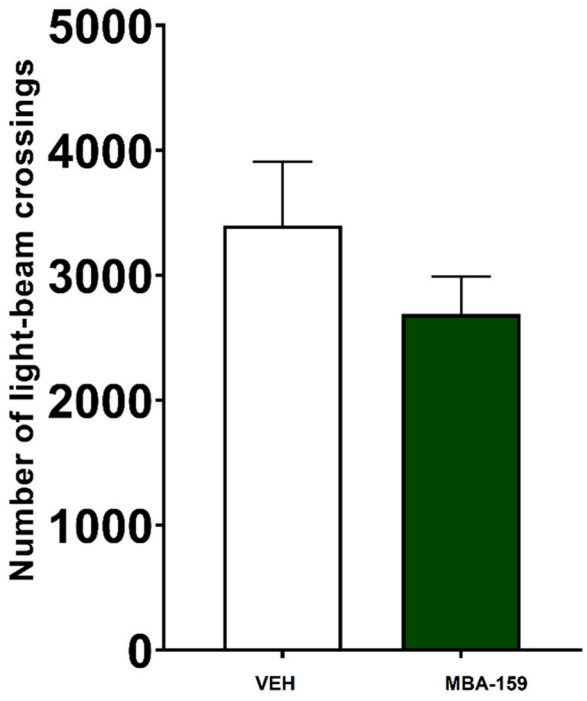


**Fig. 9.** Effect of **MBA-159** (10 mg/kg, i.p.) on locomotor activity measured in mice. Results are shown as the mean number of light-beam crossings ± SEM measured during the 30-min test for n = 10. Statistical analysis: Student's *t*-test. Significance *vs.* control: $p > 0.05$.

resembling that observed in the course of AD, we used scopolamine, a muscarinic receptor antagonist which is regarded as a 'gold standard' pharmacological tool to induce cognitive decline in rodents [35] as also shown in our previous research [36].

For the assessment of potential procognitive properties of **MBA-159,** we used two behavioural assays. These assays were selected based on the available literature data, which showed that these tests are complementary to each other as they utilize distinct stimuli, and thus, they can assess various types of memory functions in mice. These tasks enabled to assess the impact of **MBA-159** on animals' learning skills (memory acquisition) and memory retention.

PA is a fear-motivated task, and it uses an aversive stimulus (i.e., a foot shock) to assess long-term, contextual memory based on negative reinforcement. It is a fear-motivated avoidance task, which is one of the most widely used behavioural methods to measure the cognitive abilities of drugs and drug candidates in rodents. PA task is a very powerful tool for assessing the effects of drugs on memory consolidation [37]. The results obtained in the PA task revealed significant prolongation of the retention trial step-through latency (in comparison to that of the acquisition trial) in vehicle-treated mice. This indicates unimpaired learning and memory in these mice. The comparison of the retention trial step-through latency of vehicle-treated mice and the retention trial latency of mice treated with combined scopolamine and vehicle showed learning deficits in the latter group. In contrast to this, mice treated with **MBA-159** at doses 5 and 10 mg/kg demonstrated prolonged step-through latency compared to scopolamine + vehicle-treated mice. The highest dose of **MBA-159** (30 mg/kg) was not effective in this assay.

In contrast to the PA task, the NOR task relies mainly on a rodent's innate exploratory behaviour. In this task, using any external reinforcement is not required. It can measure visual memory, working memory, attention and preference for novelty in rodents [38]. The NOR task is a behavioural method for testing neurobiological aspects of nonspatial memory in mice and rats and it is based on the natural tendency of rodents to explore novel objects and the preference to explore the novel object in the recognition (T2) phase reflects a positive effect of a test compound on learning and memory [39–44]. This task revealed significant procognitive properties of **MBA-159**. We showed significant anti-amnesic properties of doses 5, 10 and 30 mg/kg of **MBA-159,** which was able to reverse visual memory impairments induced by scopolamine.

Preliminary safety pharmacology study for **MBA-159** was carried out using behavioural tests. We performed the locomotor activity test and the rotarod test to assess if **MBA-159**-exposed mice display any motor deficits. In general, **MBA-159** was safe. Also, it has to be noted that immediately after **MBA-159** administration, the mice were thoroughly observed for changes in their general condition (posture, movement, respiration, body temperature), self-maintenance behaviours, incuding grooming behaviour and coat condition, and natural behaviors like nesting, burrowing, exploration, and social interaction. Monitoring of

body weight, food and water intake, and facial expressions (the Mouse Grimace Scale) to detect pain or distress were also done. No seizure episodes were noted after **MBA-159** injection. Taken together, these parameters provided a reliable picture of the animals' well-being after **MBA-159** administration. This *in vivo* observation proved that **MBA-159** is not likely to be toxic to experimental animals but we are aware that further experimental studies (e.g. histopathological evaluations) might be necessary to confirm the safety profile of **MBA-159** in the future.

#### 2.5.3. Treatment with Contilisant and MBA-159 rescued cognitive decline in SAMP8 mice

Spatial memory, a critical cognitive function, has been increasingly recognized as an early indicator of AD [45], which was investigated by performing the object location test (OLT). Importantly, it was found that the treatment with both **Contilisant** and **MBA-159** at 10 mg/kg had a beneficial effect on the cognition of mice compared to the SAMP8 Control group (Fig. 10).

#### 2.5.4. Impact of Contilisant and MBA159 on neuroinflammation and oxidative stress markers in SAMP8 mice

Neuroinflammation, oxidative stress, and reactive gliosis are prominent pathological features of AD [46]. Therefore, RT-PCR analysis was performed using mRNA from SAMP8 mouse hippocampi to evaluate the effect of **Contilisant** and **MBA-159** treatment on these molecular key events. Firstly, we evaluated neuroinflammatory markers such as *Glial fibrillary acidic protein (Gfap)*, *Tumour necrosis factor α (Tnf-α), and Triggering receptor expressed on myeloid 2 (Trem2)*. Thus, we found a decrease in *Gfap* gene expression in both treated groups compared to the SAMP8 control mice group but did not reach statistical significance (Fig. 11A). In contrast, *Tnf-α* gene expression was lower in mice treated with **MBA-159** at 10 mg/kg and significantly lower in **Contilisant**--treated mice than control SAMP8 mice (Fig. 11B). Likewise, *Tnf-α* gene expression did not differ between **Contilisant** and **MBA-159**-treated mice. *Trem2* gene expression, however, was significantly decreased in both treated groups compared to the SAMP8 control group (Fig. 11D). Contrarily, *Superoxide dismutase 1 (Sod1)* gene expression was unaltered in SAMP8 mice whether treated with **Contilisant**, **MBA-159** or vehicle (Fig. 11C).

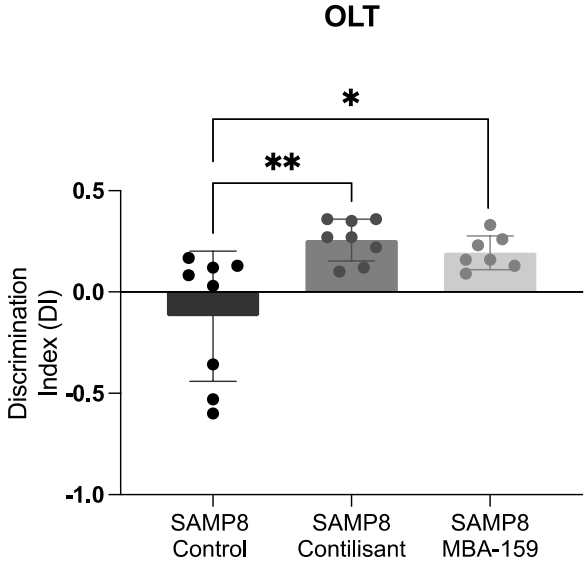


**Fig. 10.** Rescued cognitive decline in SAMP8 mice after **Contilisant** and **MBA-159** treatment. The discrimination index (DI) was determined for the OLT. The values are given as mean ± SEM. Groups were compared using one-way ANOVA analysis followed by Tukey's *post hoc* test. n = 8 per group; * $p < 0.05$; ** $p < 0.01$.

#### 2.5.4.1. Changes in memory-related genes after Contilisant and MBA-159 treatment in SAMP8 mice.

RT-PCR analysis of genes related to memory, synaptic plasticity and learning was performed to validate the improvement in cognition after both treatments. In the case of the gene expression levels of *Brain-derived neurotrophic factor (Bdnf)* mRNA in SAMP8 mouse hippocampi did not differ among the SAMP8 control group, **Contilisant**-treated and **MBA-159**-treated mice (Fig. 12A). Likewise, although no difference was observed in *Forhead box protein P2 (Foxp2)* expression in the hippocampus among the SAMP8 control group, **Contilisant**-treated and **MBA-159**-treated mice, the **MBA-159** presented a clear tendency to increase it (Fig. 12B). Furthermore, there was a significant rise in *Activity-regulated cytoskeleton-associated protein (Arc)* expression in the hippocampus after **Contilisant** at 10 mg/kg treatment but no changes in **MBA-159** treated mice group (Fig. 12C). We also evaluated the *Catechol-o-methyltransferase (Comt)* gene expression in the hippocampus of SAMP8. We showed a clear tendency to increase in the **MBA-159**-treated group compared to the SAMP8 control group (Fig. 12D). Meanwhile, no change in **Contilisant**-treated groups was found. Overall, changes in plasticity genes were observed in both treated groups but in different genes, and this might be a potential explanation for the observed *in vivo* cognitive improvement exerted by both studied compounds.

## 3. Conclusions

In this work, we have described the molecular modelling studies that have prompted us to select and propose **MBA-159** as a new polyfunctionalized MSM for the potential AD treatment.

First of all, and based on the computational analysis (see Supporting Information),we were obviously aware that the predicted results from the molecular modelling studies favored also not only the benzimidazole **7**, but the investigation of the benzoxazole **5** (Fig. 2). However, we have given preference to benzimidazole **7**, based on the large literature [20] available showing that the benzimidazole is a more real privileged scafold in the medicinal chemistry compared with the benzoxazole motif [47]. Thus, the heterocyclic benzimidazole has been largely employed in organic synthesis, has been proven to have minimal toxicity and a number of biological activities, as antifungal, antibacterial, antiviral, antituberculosis, and antiprotozoal, a capacity possibly due to its unusual structure, promoting hydrophobic interactions between enzymes and receptors through non-covalent interactions, including van der Waals, electrostatic, hydrogen bonds, coordination bonds, and π–π stacking [48]. Nevertheless, a deep similar study on benzoxazole **5** is being carried out in our laboratories and will be reported in due course.

Next, we investigated the *in silico* and *in vitro* ADMET properties, confirming that from the point of view of solubility, neurotoxicity and hepatotoxicity ligand **MBA-159** showed an excellent ADME and safety profile. Next, we conducted the *in vitro* pharmacological evaluation of compound **MBA-159** and compared it with **Contilisant**. The *in vivo* part of this research revealed that **MBA-159** possessed antiamnesic properties in a mouse model of amnesia caused by scopolamine. **MBA-159** significantly improved nonspatial (contextual and recognition) memory.

AD is characterized by progressive cognitive decline and memory loss, which have significant societal and economic impacts. The senescence-accelerated prone mouse 8 (SAMP8) strain is a valuable model for studying AD due to its early onset of learning and memory deficits, which are accompanied by AD-related brain alterations, such as increased oxidative stress and tau phosphorylation. This model enables for the evaluation of potential therapeutic interventions designed to mitigate cognitive decline and neurodegeneration [49]. Remarkably, the SAMP8 model was selected over more recent transgenic models (3xTg, APP/PS1) because it represents sporadic AD pathogenesis, which accounts for over 97 % of human AD cases, rather than the rare familial forms modeled by transgenic mice. SAMP8 mice exhibit a more comprehensive suite of human AD-relevant pathologies, including neuronal cell death—a feature typically absent in familial AD

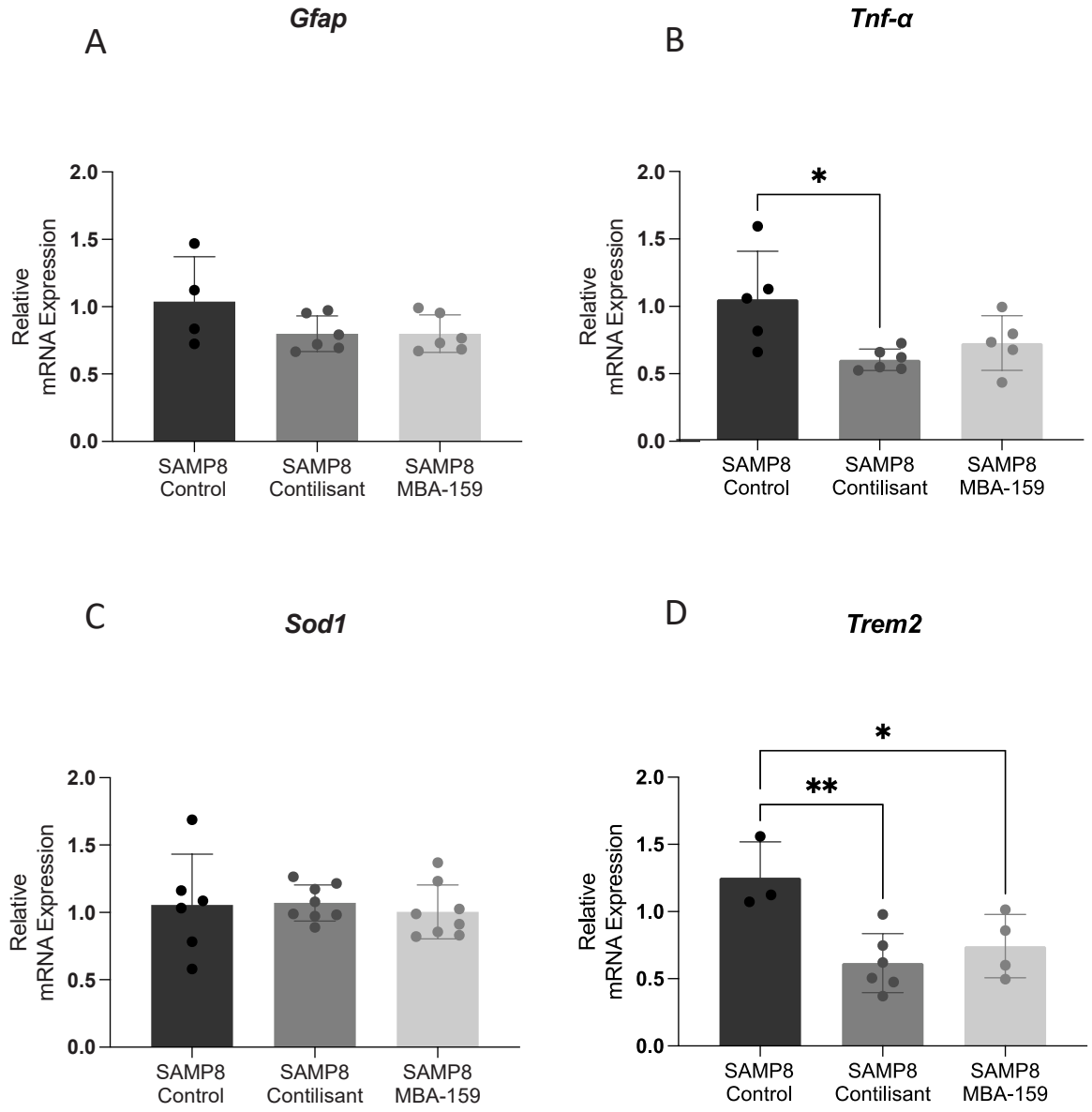


**Fig. 11. Contilisant** and **MBA-159** Treatment cause downregulation of several neuroinflammatory genes in SAMP8 mice. (A) *Gfap,* (B) *Tnf-α,* (C) *Sod1,* (D) *Trem2*. The values are given as mean ± SEM. Groups were compared using one-way ANOVA analysis followed by Tukey's *post hoc* test. n = 4–6 per group; * $p < 0.05$; ** $p < 0.01$.

models—along with vascular pathology, extensive neuroinflammation, and metabolic alterations that mirror the progression of human sporadic disease [50].

Both treatments showed a trend towards reducing *Gfap* gene expression, although not statistically significant. However, **Contilisant** significantly reduced *Tnf-α* expression, suggesting a more potent anti-inflammatory effect compared to that of **MBA-159**. *Trem2* gene expression was also significantly decreased in both treated groups, indicating their potential role in modulating microglial activation. These findings align with previous research showing that reducing neuroinflammation can mitigate AD pathology. The lack of change in *Sod1* gene expression suggests neither treatment directly impacts oxidative stress, consistent with some studies showing that oxidative stress might not be the primary target for these compounds. **Contilisant** significantly increased *Arc* expression, a key regulator of synaptic plasticity, indicating its potential to enhance memory consolidation and synaptic function. This effect was not observed with **MBA-159**, which showed a tendency to increase *Foxp2* and *Comt* expression, suggesting different mechanisms of action.

In this context, it is very interesting to highlight that it has not been surprising to find the very promising and attractive biological properties described herein for compound **MBA-159**, as this molecule bears a benzimidazole motif, a particularly gifted and privileged heterocyclic scafold in medicinal chemistry [20], that is present for instant in compound **AZP2006** [51] (Fig. 13), a candidate in advanced in clinical phase for the therapy of progressive supranuclear palsy (PSP), able to efficiently address lysosomal dysfunction and tau pathologym representing thus a new disease-modifying approach for PSP and other neurodegenerative disorders, such as AD and Parkinson' s disease. This is also the case of benzimidazoles reported by Decker and colleagues [52], among them, the most promising compound **11d** (Fig. 13) was shown to attenuate $A\beta_{25-35}$-induced learning impairments in both spontaneous alternation and PA responses at low 0.03 mg $kg^{-1}$ dose, providing selective BuChE inhibition, leading thus to efficient neuroprotectivity in AD.

In summary, our findings indicate that **Contilisant** and **MBA-159**

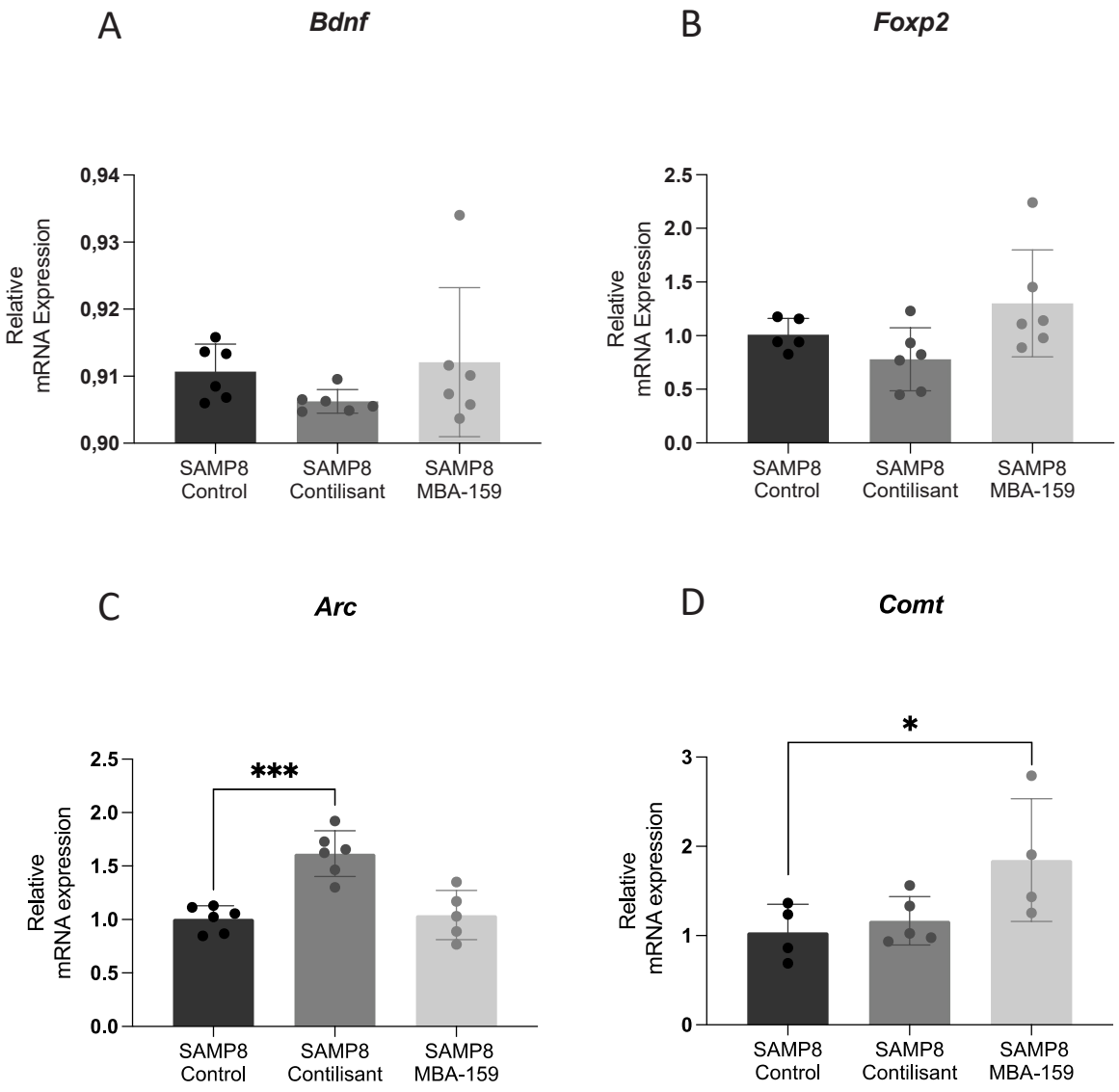


**Fig. 12. Contilisant** and **MBA-159** treatment caused upregulation of synaptic plasticity genes in SAMP8 mice. (A) *Bdnf,* (B) *Foxp2,* (C) *Arc,* (D) *Comt*. The values are given as mean ± SEM. Groups were compared using one-way ANOVA analysis followed by Tukey's *post hoc* test. n = 4–6 per group; *** $p < 0.001$.

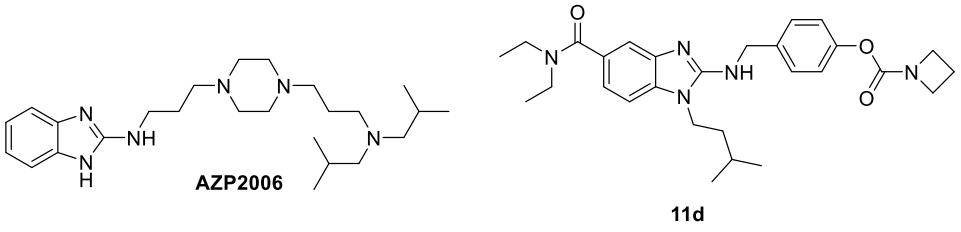


**Fig. 13.** Structures of benzimidazoles **AZP2006**, and **11d**.

have distinct effects on neuroinflammation and synaptic plasticity in the SAMP8 mouse model of AD. **Contilisant**'s ability to significantly reduce *Tnf-α* and increase *Arc* expression suggests a more comprehensive approach to addressing AD pathology, potentially offering a novel therapeutic avenue. However, further studies are needed to elucidate the precise mechanisms and long-term effects of these treatments on AD progression. Taken together, ligand **MBA-159** can be considered a new lead compound for further extended studies focused on searching for novel therapies for AD.

## 4. Experimental part

### 4.1. Molecular docking

The structure of compound **MBA-159** and **Contilisant** were constructed as hydrochlorides and free amines using build option within Discovery Studio (DS 2022). A single low-energy 3D conformation was generated by energy minimization using the adopted Newton-Raphson algorithm with the CHARMm force field [53]. The coordinates of hAChE (PDB ID: 1B41) and hBuChE (PDB ID: 4BDS) were obtained from

the Protein Data Bank. Using protein model tool in DS software package, proper bonds, bond orders, hybridization and charges were assigned. Three-dimensional crystal structure of the hS1R receptor bound to the antagonist PD144418 (PDB: 5HK1) was retrieved from the Protein Data Bank (PDB). Chain B of the receptor was extracted only from the 5HK1 structure for further modeling. The crystal structure of hH3R (PDB ID: 7F61) is used and DS prepared it. The identification of an appropriate docking protocol is a key step in the obtaining of reliable docking poses. Hence, the reliability of the docking method was determined by the resemblance of the docked conformation with the co-crystallized PF03654746 (RMSD of 0.615 Å). In the crystallized proteins, cocrystal ligands and water molecules were removed and initial proteins were prepared for docking purposes using AutoDockTools (ADT; version 1.5.7) to add hydrogens and partial charges for proteins and ligands using Gasteiger charges. Flexible torsions in the ligands were assigned with the AutoTors module, and the acyclic dihedral angles were allowed to rotate freely. For hAChE eight residues were allowed to move using the AutoTors module: Trp286, Tyr124, Tyr337, Tyr341, Tyr72, Asp74, Thr75, Trp86. The grid box was built with a resolution of 1 Å and 60 × 60 × 72 points and it was positioned at the middle of the protein (x = 116.546; y = 110.33; z = -134.181). In the case of H3R, Tyr91, Tyr94, Trp110, Tyr115, Tyr189, Tyr374, Tyr394 and Phe398 receptor residues were selected to keep flexible during docking. 44 × 72 × 46 with grid points separated 1 Å was positioned in the middle of the protein (x = -20.587; y = 30.520; z = 0.997). For hS1R, we have chosen as flexible twelve amino-acids side chains: Tyr103, Glu172, Phe107, Asp126, Val152, Phe146, Gln135, His154, Glu158, Ser117, Tyr120 and Tyr206. The docking box was positioned at the middle of the protein (x = -6.978; y = 20.413; z = -27.539). A grid box of 28 × 22 × 34 with grid point spacing of 1 Å, was used. For hBuChE, a grid box of 66 × 60 74 with grid points separated 1 Å was positioned in the middle of the protein (x = 136.0; y = 123.59; z = 38.56). For MAO-A, the grid center coordinates were x = 53.065, y = 161.664, z = 26.000 and the size coordinates were x = 24, y = 34, z = 38 with grid points separated 1 Å; for MAO-B, the grid center coordinates were x = 53.065, y = 161.664, z = 29.046 and the size coordinates were x = 24, y = 34, z = 36 with grid points separated 1 Å. All docking calculations were performed with the program AutoDock Vina [19] and they were applied to the whole protein target (blind docking). The first-ranked binding poses for the ligand in the active-site gorge of ChEs, MAO-A, MAO-B, S1R and H3R were adopted in the present work for further analysis with DS.

### 4.2. In silico ADME profiling

ADME properties of **MBA-159** were calculated using the QikProp module of Schrodinger suite (QikProp, Schrödinger, LLC, New York, NY, 2022] running in normal mode.

### 4.3. Synthesis of MBA-159

#### 4.3.1. General methods

The experimental procedures were carried out in an inert atmosphere by using Schlenk techniques unless otherwise stated. All chemical reagents and solvents were purchased from Acros Organics, Sigma-Aldrich, Alfa Aesar, TCI, or Fluorochem. NMR spectra were recorded on a Varian Mercury Plus 300 multinuclear spectrometer at 300 MHz ($^1$H NMR) and 75 MHz ($^{13}$C NMR), a Bruker AVANCE Neo 400 Nanobay at 400 MHz ($^1$H NMR), and 101 MHz ($^{13}$C NMR), a Varian NMR System 500 multinuclear spectrometer at 500 MHz ($^1$H NMR), and 126 MHz ($^{13}$C NMR). The assignment of chemical shifts was based on standard NMR experiments ($^1$H, $^{13}$C, $^1$H-$^1$H COSY, $^1$H-$^{13}$C HSQC and $^1$H-$^{13}$C HMBC) using solvent peaks [$CDCl_3$:7.27 (D), 77.2 (C) ppm and DMSO-$d_6$ 2.50 (D) and 39.7 (C) ppm] as internal references. Coupling constants (J) are given in Hertz and signals are described as follows: s, singlet; d, doublet; t, triplet; q, quadruplet; bs, broad singlet; bd, broad doublet; dd, double doublet; ddd, double doublet of doublets; tt, triple triplet and m, multiplet. High-resolution mass spectra analyses (HRMS) were performed on a Triple TOF 5600 plus Sciex LC/MS. IR spectra were measured on an FT-IR spectrometer in an ATR mode. Melting points were determined in a Koffler apparatus, and are uncorrected. Reactions were monitored using analytical TLC plates (Scharlab; silica gel 60 F254, 0.20 mm) visualized by UV-light at 254 and 365 nm and the purification of the products was carried out in Biotage isolera one flash chromatography instrument.

**5-Hydroxy-1-methyl-1*H*-benzo [*d*] imidazole-2-carbaldehyde** (**13**). To a solution of compound **12** [27] (1 g, 5.26 mmol) in dry DCM (40 mL), a solution of $BBr_3$ (1.5 mL, 15.8 mmol, 3 equiv) in dry DCM (10 mL) was added dropwise, under argon, at −75 ºC. The reaction mixture was stirred at –75 ºC for 30 min, and for 1 h at rt. Once the reaction has been completed (TLC analysis), some drops of distilled water were added, and when the effervescence ceased, aq $NH_4OH$ was added until pH 7–8 and a yellow solid was formed, that was filtered and dried to obtain compound **13** (767 mg, 82 %) as beige solid ($R_f$= 0.33, DCM/MeOH, 10 %): $^1$H NMR (300 MHz, DMSO-$d_6$) δ 9.92 (s, 1 H), 9.46 (s, 1 H), 7.54 (d, *J*= 8.9 Hz, 1 H), 7.19 – 6.73 (m, 2 H), 4.02 (s, 3 H).

**1-Methyl-2-((methylamino)methyl)-1*H*-benzo [*d*] imidazol-5-ol** (**14**). To a suspensión of compound **13** (767 mg, 4.35 mmol) and $Na_2SO_4$ (4.95 g, 34.9 mmol, 8 equiv) in dry DCM (16 mL) a solution of methylamine solution (2.0 M) in MeOH (4.35 mL, 8.7 mmol, 2 equiv) was added. Then, $Na_2SO_4$ was filtered, and washed with DCM. The organic layer was dissolved in MeOH (15 mL) and treated with $NaBH_4$ (137 mg, 3.44 mol, 1.1 equiv), under argon, at 0 ºC and stirring at rt for 2 h. Then, some drops of distilled water were added and the solvent was evaporated under reduced pressure. The solid was purified by flash column chromatography (DCM/MeOH 0–5 %) to obtain compound **14** (583 mg, 70 %) as white solid ($R_f$= 0.25, DCM/MeOH, 10 %): mp: 162–164 ºC, IR (ATR) v 3179, 2948, 2799, 1623, 1591, 1485, 1442, 1408, 1254, 1169, 1101 cm$^{-1}$. $^1$H NMR (300 MHz, DMSO-$d_6$) δ 8.92 (s, 1 H), 7.24 (d, *J*= 8.6 Hz, 1 H), 6.87 (d, *J*= 2.2 Hz, 1 H), 6.68 (dd, *J*= 8.6, 2.2 Hz, 1 H), 3.81 (s, 2 H), 3.70 (s, 3 H), 2.28 (s, 3 H); $^{13}$C NMR (101 MHz, DMSO-$d_6$) δ 153.7, 153.1, 143.2, 130.3, 111.7, 110.1, 103.8, 48.0, 36.3, 30.0. HRMS (ESI) Calcd. for $C_{10}H_{13}N_3O$ (M+H): 192.11314. Found: 192.11316.

**1-Methyl-2-((methyl(prop-2-yn-1-yl)amino)methyl)-1*H*-benzo [*d*] imidazol-5-ol** (**15**). To a solution of compound **14** (583 mg, 3.05 mmol) in dry THF (15 mL), propargyl bromide (0.51 mL, 4.58 mmol, 1.5 equiv) and DIPEA (0.79 mL, 4.58 mmol, 1.5 equiv) were added dropwise, under argon at 0 ºC. Then, the reaction mixture was stirred at rt overnight, and the solvent was evaporated under reduced pressure. The crude solid was purified by flash column chromatography (DCM/MeOH from 0 % to 5 %) to obtain compound **15** (525 mg, 75 %) as white solid ($R_f$= 0.41, DCM/MeOH, 5 %): mp: 176–178 ºC, IR (ATR) v 3283, 2942, 2853, 2793, 2107, 1623, 1591, 1483, 1438, 1407, 1351, 1328, 1157, 1028 cm$^{-1}$. $^1$H NMR (400 MHz, DMSO-$d_6$) δ 8.97 (s, 1 H), 7.28 (d, *J*= 8.6 Hz, 1 H), 6.91 (d, *J*= 2.0 Hz, 1 H), 6.73 (dd, *J*= 8.6, 2.0 Hz, 1 H), 3.74 (s, 3 H; s, 2 H: 5 H), 3.37 (d, *J*= 2.3 Hz, 2 H), 3.24 (t, *J*= 2.3 Hz, 1 H), 2.23 (s, 3 H); $^{13}$C NMR (101 MHz, DMSO-$d_6$) δ 153.2, 151.8, 143.1, 130.4, 112.1, 110.3, 103.9, 79.1, 76.7, 52.3, 45.4, 41.5, 30.2. HRMS (ESI) Calcd. for $C_{13}H_{15}N_3O$ (M+H): 230.12879. Found: 230.12876.

***N*-Methyl-*N*-((1-methyl-5-(3-(piperidin-1-yl)propoxy)-1*H*-benzo [*d*] imidazol-2-yl)methyl)prop-2-yn-1-amine** (**MBA-159**). To a solution of compound **15** (525 mg, 2.29 mmol) in dry DMF (5 mL), NaH (206 mg, 5.15 mmol, 2.25 equiv) was added, under argon, at 0 ºC. The reaction mixture was stirred for 10 min; then, 1-(3- chloropropyl) piperidine hydrochloride (499 mg, 2.52 mmol, 1.1 equiv) was added and the mixture stirred overnight at rt. The solvent was evaporated and purified by flash column chromatography (DCM/MeOH 0–10 %) to obtain **MBA-159** (310 mg, 38 %) as a beige solid ($R_f$= 0.45, DCM/MeOH, 10 %): mp: 180–182 ºC; IR (ATR) v 2944, 2918, 2870, 2801, 2107, 1617, 1595, 1489, 1438, 1407, 1217, 1026 cm$^{-1}$; $^1$H NMR (500 MHz, DMSO-$d_6$) δ 7.37 (d, *J*= 8.8 Hz, 1 H, H7-benzimidazole),

7.09 (d, *J*= 2.3 Hz, 1 H, H4-benzimidazole), 6.85 (dd, *J*= 8.8, 2.3 Hz, 1 H, H6-benzimidazole), 3.99 (t, *J*= 6.4 Hz, 2 H, $CH_2O$), 3.76 [s, 5 H, (3H-benzimidazole-N($CH_3$)+2H-benzimidazole-$CH_2$)], 3.36 [d, *J*= 2.3 Hz, 2 H, $CH_2N(CH_3)CH_2C{\equiv}CH$], 3.23 [t, *J*= 2.4 Hz, 1 H, $CH_2N(CH_3)CH_2C{\equiv}CH$], 2.44 – 2.29 [m, 6 H, (2H-$CH_2CH_2CH_2O$+4H-N($CH_2$)$_2$)], 2.22 [s, 3 H, $CH_2N(CH_3)CH_2C{\equiv}CH$], 1.90 – 1.81 (m, 2 H, $CH_2CH_2CH_2O$), 1.53 – 1.44 [m, 4 H, N($CH_2$)$_2$ ($CH_2$)$_2$], 1.41–1.33 [m, 2 H, N($CH_2$)$_2$ ($CH_2$)$_2CH_2$]; $^{13}$C NMR (126 MHz, DMSO-$d_6$) δ 155.0 (C-5), 152.1 (C-2), 143.0 (C-3a), 131.2 (C-7a), 112.5 (C-6), 110.6 (C-7), 102.9 (C-4), 79.1 ($NCH_2C{\equiv}CH$), 76.7 ($NCH_2C{\equiv}CH$), 66.9 ($OCH_2$), 55.7 ($CH_2CH_2CH_2O$), 54.5 [N($CH_2$)$_2$], 52.3 ($CH_2N(CH_3)CH2C{\equiv}CH$), 45.4 ($CH_2N(CH_3)CH_2C{\equiv}CH$), 41.5 [$CH_2N(CH_3)CH_2C{\equiv}CH$], 30.3 [benzimidazole-N($CH_3$)], 26.8 ($CH_2CH_2CH_2O$), 25.9 [N($CH_2$)$_2$($CH_2$)$_2$], 24.5 [N($CH_2$)$_2$ ($CH_2$)$_2CH_2$]. HRMS (ESI) [M+H]: Calcd. for $C_{21}H_{30}N_4O$: 354.2420. Found: 354.2419.

### 4.4. Preliminary in vitro ADMET profiling for MBA-159

#### 4.4.1. Metabolic stability assay

Metabolic stability was assessed using liver microsomes, pooled from mouse (CD-1), male, Sigma-Aldrich. Incubations were carried out in 96-well plates. Potassium phosphate buffer (100 mM, pH 7.4, 2 mM $MgCl_2$), containing mouse liver microsomes (0.5 mg protein/mL), was pre-incubated with test compounds or positive control (1 μM) at 37 °C for 10 min (n = 2). Reactions were initiated by adding NADPH (1 mM). To exclude non-NADPH metabolism or chemical instability in the incubation buffer, reactions were also incubated without NADPH. The reactions were terminated after 15 min by the addition of an acetonitrile quenching solution containing an internal standard (labetalol, 0.5 mM). The plates were centrifuged at 4000 rpm for 30 min at 4 °C, and an aliquot of supernatant was diluted with water before analysis by UPLC-MS/MS. The UPLC-MS/MS system consisted of a Waters Acquity Premier (Waters Corporation, Milford, MA, USA) coupled to a Waters Xevo TQ-S Cronos mass spectrometer (electrospray ionization mode ESI). Chromatographic separations were carried out using the Acquity UPLC BEH (bridged ethylene hybrid) C18 column; 2.1 × 100 mm, and 1.7 μm particle size, equipped with Acquity UPLC BEH C18 VanGuard pre-column; 2.1 × 5 mm, and 1.7 μm particle size. The column was maintained at 40 °C, and eluted under gradient conditions using from 95 % to 0 % of eluent A over 10 min, afterwards 100 % of eluent B over 2.5 min, at a flow rate of 0.3 mL min-1. Eluent A: water/formic acid (0.1 %, v/v); eluent B: acetonitrile/formic acid (0.1 %, v/v). Chromatograms were recorded using Waters eλ PDA detector. Spectra were analyzed in 200–700 nm range with 1.2 nm resolution and sampling rate 20 points/s. MS detection settings of Waters Xevo TQ-S Cronos mass spectrometer were as follows: source temperature 150 °C, desolvation temperature 250 °C, desolvation gas flow rate 600 L $h^{-1}$, cone gas flow 100 L $h^{-1}$, capillary potential 3.00 kV, cone potential 30 V. Nitrogen was used for both nebulizing and drying gas. The data were obtained in a scan mode ranging from 50 to 1000 m/z in time 0.5 s intervals. Data acquisition software was MassLynx V 4.2 (Waters). The peak area ratios of analyte versus internal standard were used to calculate the percentage remaining of the test compound (%).

#### 4.4.2. Thermodynamic solubility assay

The quantitative HPLC analyses were acquired using Waters Alliance e2695 separations module (Waters, Milford, CT, USA) containing 2998 photodiode array (PDA), a detector (Waters, Milford, CT, USA), and the SpeedROD RP-18e 50 −4.6 mm column (Merck, KGaA, Darmstadt, Germany). The temperature of the column was preserved at 30 °C. The experiment was conducted under the following conditions: a flow rate of 5 mL $min^{-1}$, eluent A (water/0.1 % HCOOH), eluent B (MeCN/0.1 % HCOOH), a gradient starting from 0 % of B to 100 % of B over a duration of 3 min. Each sample was injected at a volume of 10 μL in triplicate, and the spectra were analysed at maximum wavelength. Standard solutions for the calibration curve were prepared in methanol with concentrations ranging from 0.02 to 2 mg/mL, and they were quantified by HPLC. The calibration curve was plotted using the area under the curves (AUC) against concentration (mg/mL). Next, 2 mg of the tested compound was dissolved in 1 mL of Dulbecco's phosphate-buffered saline (DPBS), and the mixture was constantly agitated at 20 °C for 24 h in a thermoshaker. After that time, the mixture was filtered through a cellulose acetate syringe filter (pore size 0.22 μm) and solution was analyzed by HPLC. Solubility of the tested compound was calculated using the calibration curve (mg/mL).

#### 4.4.3. Neurotoxicity and hepatotoxicity

Neurotoxicity was evaluated using the human neuroblastoma cell line SH-SY5Y (ATCC® no. CRL-2266™). Cells were seeded (5 ×$10^3$ cells/100 μl/well) in transparent 96-well plates (FALCON no. 353072, Corning, USA) in DMEM/F12 (Gibco no. A41920–01) supplemented with 10 % FBS (Gibco no. 10500–064) and cultured overnight. The next day, the medium was removed and replaced with a fresh one that contained: 1) dimethylsulfoxide (DMSO < 0.1 %, vehicle control (Veh)); 2) increasing concentration of the compound **MBA-159** (0.75, 1, 5, 10, 25, 50, 100 μM); 3) doxorubicine (DOX, 0.75, 1, 5, 10, 25, 50, 100 μM). Treatment with compounds was carried out for 72 h. During this time, cells were examined under inverted microscope for precipitates in the medium. Cell viability was examined using an MTS-based CellTiter96® AQueous One Solution Cell Proliferation Assay (Promega, Madison, WI, USA) following the manufacturer's protocol. The absorbance was measured at 490 nm using the Tecan Spark multimode plate reader (Tecan, Männedorf, Switzerland). A reference wavelength of 630 nm was used to subtract the background. $IC_{50}$ values were calculated by fitting a nonlinear regression to a sigmoidal dose-response curve in GraphPad Prism version 8.0.1. Hepatotoxicity was evaluated with the MTS assay. Cells were seeded (15 ×$10^3$ cells/100 μL/well) in transparent 96-well plates (FALCON no. 353072, Corning, USA) in DMEM (Gibco no. 61965–026) supplemented with 10 % FBS (Gibco no. 10500–064) and cultured overnight. The next day, the medium was removed and replaced with a fresh one that contained: 1) dimethylsulfoxide (DMSO < 0.1 %, vehicle control (Veh)); 2) increasing concentration of the compound **MBA-159** (0.75, 1, 5, 10, 25, 50, 100 μM); 3) doxorubicine (DOX, 0.75, 1, 5, 10, 25, 50, 100 μM). Treatment with compounds was carried out for 72 h. The cell viability assay was performed as described above (neurotoxicity part).

### 4.5. In vitro analysis of MBA-159

#### 4.5.1. Inhibition of cholinesterases

[30]. The inhibitory potencies of the compounds against the cholinesterases were determined by the method of Ellman. Briefly, compounds were incubated with Ellman's reagent (final concentration, 370 μM) and the ChEs (final concentration, approx. 1 nM or 100 pM hBuChE or hAChE, respectively) in 0.1 M sodium phosphate (pH 8.0) for 5 min at 20 °C on 96-well microplates. Reactions were started adding the substrate (final concentration, 500 μM butyrylthiocholine iodide [BTCI] or acetylthiocholine iodide [ATCI] for hBChE and hAChE, respectively). The final content of DMSO was always 1 % (v/v). The increase in absorbance (λ = 412 nm) was monitored for 2 min using a microplate reader (Tecan Spark microplate reader, Tecan, Switzerland). The initial velocities in the presence ($v_i$) and absence ($v_o$) of the compounds were calculated, and the inhibitory potencies were expressed as residual activities (RA = $v_i$ / $v_o$). The $IC_{50}$ values were calculated in GraphPad Prism 9.3 software (4-parameter logistic function; GraphPad Software, USA). Donepezil was used as a positive control.

#### 4.5.2. Inhibition of MAO A/B

[30]. Recombinant microsomal hMAOs expressed in BTI-TN-5B1–4 cells, HRP (type II, lyophilized powder), *p*-tyramine hydrochloride and Amplex Red were purchased from Sigma Aldrich (Sigma Aldrich, MO, USA). Briefly, 100 μL of 50 mM sodium phosphate (pH 7.4, 0.05 % [v/v]

Triton X-114) containing the test compounds, and hMAO-A or hMAO-B were incubated at 37 °C for 15 min in 96-well microplates (Nunc Microwell microplates, Thermo Fisher). After preincubation, the reaction was started by adding Amplex Red (final concentration, 200 μM), HRP (2 U/mL), and *p*-tyramine (1 mM). The increase in fluorescence intensity ($\lambda_{ex}$ = 530 nm, $\lambda_{em}$ = 590 nm) was monitored at 37 °C for 30 min using a microplate reader (Tecan Spark microplate reader, Tecan, Switzerland). DMSO was used for control experiments (1 %, v/v). To determine the blank value (*b*), sodium phosphate buffer replaced the enzyme solution. Initial velocities were calculated from the trends obtained, with each measurement performed in duplicate. The inhibitory potencies are expressed as the RAs according to equation: $RA = (v_i - b) / (v_o - b)$, where $v_i$ is the velocity in the presence of the test compounds, and $v_0$ is the control velocity in the presence of DMSO. The $IC_{50}$ values were calculated in GraphPad Prism 9.3 software (4-parameter logistic function; GraphPad Software, USA).

#### 4.5.3. DPPH radical-scavenging potency

[30]. Free-radical scavenging potency was evaluated using the DPPH assay. DPPH (2,2-diphenyl-1-picrylhydrazyl radical) was dissolved in MeOH (150 μL, 140 μM) and added to 150 μL methanol solution of the test sample (screening at 100 μM, serial dilution of compounds for $EC_{50}$ determination) or methanol (negative control) on 96-well microtiter plates (Brand microplate, pureGrade, F-bottom). The microtiter plate was incubated at room temperature in the dark for 90 min. The absorbance at 517 nm was determined with a microplate reader (Tecan Spark microplate reader, Tecan, Switzerland). The experiments were performed in triplicate, with subtraction of the blank value (compound without DPPH). The percentages of DPPH free radicals were calculated as DPPH free radical (%) = $[(A_0 - A_1) / A_0] \times 100$, where $A_0$ is the absorbance of the negative control, and $A_1$ is the absorbance of the test sample. Resveratrol and Trolox were used as the positive controls under the same assay conditions.

#### 4.5.4. In vitro $A\beta_{1-42}$ aggregation inhibition – Thioflavin-t (ThT) assay

[31]. Briefly, HFIP-pretreated $A\beta_{1-42}$ (1.5 μM), **MBA-159** and ThT at 10 μM were incubated in 96-well microplate at rt in quadriplicates with shaking for 48 h. The fluorescence ($\lambda$ = 440/490 nm) was measured every 10 min (Tecan Spark microplate reader, Tecan, Switzerland), and the plateau fluorescence intensities with or without the compound were averaged, and the well's average fluorescence at 0 h was subtracted. The $A\beta_{1-42}$ aggregation inhibition is calculated as %Inh = $(1–F_i / F_0) \times 100$, where $F_i$ repspresent represents the fluorescence intensity of the weels in the presence of the test compound, and $F_0$ is the control fluorescence intensity.

### 4.6. In Vivo pharmacokinetic experiments

#### 4.6.1. Animal study. Experimental protocol

Pharmacokinetic experiments were performed on fifteen male Wistar rats weighing between 200 and 250 g, which were supplied from Envigo Rms Co., Ltd. (Barcelona, Spain). The study was conducted in the Animal Experimentation Centre at the University of Alcalá following the Ethical Committee Regulations of the University, Community of Madrid PROEX 369.7/21, project identification code ES280050001165 (18 November 2021). The animals were housed in standard cages in 12–h light–dark cycles and had unrestricted access to food and water throughout the experiment. Experiments were performed on two groups of animals (n = 6). Treatments of **MBA-159** and **Contilisant** raw material, equivalent to a 30 mg/kg dose, were suspended in a sodium carboxymethylcellulose solution (0.35 % w/v) and 0.4 mL of the treatments were administered to the rats through oral gavage. A control group (n = 3) received only 0.4 mL of the sodium carboxymethylcellulose solution (0.35 % w/v). Blood samples were collected from the tails of the rats at 0.5, 1, 2, 3, 5, 7 and 24 h.

#### 4.6.2. Preparation of stock solutions, working standards and analyte extraction

Stock solutions of **MBA-159** and **Contilisant** in 1 % formic acid water were prepared at a 0.4 mg/mL. A serial dilution in 1 % formic acid water was performed to produce working standards from 0.4 μg/mL to 8 μg/mL. Blank plasma was obtained from animal control group. The samples were transferred to heparinized Eppendorf tubes and centrifuged at 4500 rpm for 10 min to collect the plasma. The plasma homogenates were stored at - 20 ºC. After defrosting at room temperature, plasma aliquots were added to working standards solutions in a 3:1 proportion respectively. Consecutively, 0.3 mL of 1 % formic acid acetonitrile solution was added on 0.1 mL of plasma standards in a Phree™ Phospolipid Removal 1 mL pre-columns (Phenomexex®, USA) to obtain reference standards in a range from 30 ng/mL to 600 ng/mL. Pre-columns were vortexed at 16.000 rpm for 1 min before the filtration of the samples in a vacuum manifold system for solid-phase extraction (SPE) at 15 in. Hg for 5 min. Protein precipitation and analyte extraction from samples were performed with 300 μL of 1 % formic acid acetonitrile added to a 70 μL plasma sample, plus 30 μL of a 0.01 μL/μL solution of formic acid/water to maintain the formic acid concentrations as in the standards samples. The extractions were performed in Phree™ Phospolipid Removal 1 mL pre-columns (Phenomexex®, USA) in a vacuum manifold system at 15 in. Hg for 5 min after vortexed the samples at 16.000 rpm for 1 min.

### 4.7. In vivo analysis of MBA-159: the effect of the test compound MBA-159 on learning and memory in mice, namely PA and NOR tasks

#### 4.7.1. Materials and methods. Animals and housing conditions

In this *in vivo* study adult male Albino Swiss (CD-1) mice weighing between 18 and 22 g and purchased from the Animal Breeding Farm of the Faculty of Pharmacy, Jagiellonian University Medical College were used. Animals were housed in cages (10 mice per cage) at a constant temperature of 22 ± 2 °C, humidity of 55 ± 10 % and a light/dark (12:12) cycle. The mice had unlimited access to food and water prior to the experiment. Specified conditions for the maintenance of mice were ensured throughout the experiments, including tree bedding (Transwior, Poland) and cage enrichment (tunnels, nesting material, wooden igloos, etc.). For behavioural tests the mice were selected randomly; each group consisted of 7–12 mice. The experiments were performed between 9 AM and 3 PM. After *in vivo* tests, the animals were immediately euthanized. The procedures for maintenance and treatment of laboratory animals were approved by the 1st Local Ethics Committee in Krakow and the treatment of animals was in full accordance with ethical standards laid down in respective Polish and EU regulations (Directive 2010/63/EU).

#### 4.7.2. Drugs and dose selection for the in vivo tests

Based on the previous research [40] scopolamine hydrobromide (Sigma Aldrich, Poland) at the dose of 1 mg/kg was used to induce learning and memory deficits. For the *in vivo* tests scopolamine was prepared in distilled water (Polfa Kutno, Poland) and was administered subcutaneously (s.c.) 30 min before behavioural tests during the acquisition (training) trial of PA and NOR tasks. **MBA-159** was suspended in 1 % Tween 80 (Sigma Aldrich, Poland) and was administered intraperitoneally (i.p.) 60 min before the acquisition trial of these behavioural tasks. In the rotarod and locomotor activity tests **MBA-159** was also injected i.p. 60 min before the test. As both the PA and NOR tasks were used as screening, first-in-animal tests for the evaluation of antiamnesic properties of the test compound, in these assays procognitive activity of 3 doses of **MBA-159** were assessed, namely 5, 10 and 30 mg/kg.

#### 4.7.3. Behavioural tests

*4.7.3.1. Passive avoidance task.* In order to assess the influence of **MBA-**

**159** on fear-motivated learning and memory in mice, the PA task was conducted according to a previously described protocol used in our laboratory [40]. The PA apparatus (Panlab Harvard Apparatus, Spain) consists of a large white-colored illuminated compartment (26 cm × 26 cm × 34 cm) and a small black-colored compartment (13 cm × 7.5 cm × 7.5 cm) which are separated from each other by a guillotine gate (5 cm × 5 cm). The PA task is divided into two trials (i.e., the acquisition trial and the retention trial), each conducted 24 h apart. On the first day, during the acquisition trial (a conditioning phase), the test compounds (scopolamine, **MBA-159** and vehicle) were injected. Then, each mouse was placed into the white compartment, and a 30-s habituation period began (guillotine gate is closed). After that, the guillotine gate was opened, and the mice were tested during the 180-s testing period. As soon as the mouse entered the black compartment of the PA device, the guillotine gate was closed and an electrical shock (intensity: 0.2 mA, duration: 2 s) was automatically applied through the grid floor. For each mouse the latency between opening of the guillotine gate and mouse's entering the black compartment was measured. On the next day, during the retention (drug-off) trial, the mice were placed again into the white compartment for a 30-s habituation period and the latency to enter the black compartment was measured for each mouse. Increased latency to enter the black compartment in the retention trial in scopolamine + **MBA-159**-treated groups compared to that measured in scopolamine-treated control was considered as an indicator of the compound's antiamnesic (procognitive) properties.

*4.7.3.2. Novel object recognition task.* The protocol used to perform the NOR task for the assessment of the effect of **MBA-159** on visual memory was adapted from the work of Ennaceur and Delacour [41] and was slightly modified to use this method in mice [42]. The experiment was conducted in opaque black boxes (dimensions: 50 × 50 × 50 cm). In this task, the 3-day procedure consists of habituation to the test arena (without any objects used) for 10 min on the first day (T0), a training trial (T1) and a testing trial (T2) separated by a 24-h inter-trial interval. During T1 trial (familiarization trial), two identical objects (A and B) were presented in the opposite corners of the arena, each object was located approximately 5 cm from its walls. During T2 phase (recognition trial), one of the objects (B) was replaced by a novel object (C), so that the animals were presented with A (familiar) and C (novel) objects. Both T1 and T2 trials lasted for 10 min. After each trial the animals returned to their home cages. White plastic round containers (height 5 cm, diameter 5 cm) attached to the ground with double-sided tape were used as the A, B objects and green cuboids of similar height were used as novel (C) objects. The sequence of presentations and the location of the objects were randomly assigned to each mouse and the objects were stable enough so that the animals could not displace them. The animals explored the objects by looking, licking, sniffing, or touching them while sniffing, but not when leaning against, sitting, or standing on the objects. Any mouse exploring the two objects for less than 5 s within the 10-min duration of T1 or T2 was excluded from the study. An experimenter, blind to the drug treatment, measured the exploration time of the objects. Based on exploration time (E) of the two objects during T2, discrimination index (DI) was calculated according to the formula: DI = (EC − EA)/(EA + EC) x 100. In this task, scores approaching zero reflect no preference, while positive values reflect preference for the novel object and negative numbers reflect preference for the familiar object.

*4.7.3.3. Rotarod test.* Three days before the rotarod test, the mice were trained on the rotarod apparatus (Rotarod apparatus, May Commat RR0711, Turkey; rod diameter: 2 cm) that was rotated at a fixed speed of 18 rotations per minute (rpm). In each training session, the mice were placed on the rotating rod for 3 min with an unlimited number of trials. The proper experiment was performed 24 h after the last training trial. Sixty min after the administration of **MBA-159** or vehicle, the mice were tested on the rod that revolved at 6, 18, and 24 rpm. Motor impairments in mice were defined as the inability to remain on the rotarod apparatus for 1 min. The results are expressed as the mean time spent on the rotarod [43].

*4.7.3.4. Locomotor activity test.* The locomotor activity test was performed using activity cages (40 cm x 40 cm x 30 cm, supplied with I.R. beam emitters) (Activity Cage 7441, Ugo Basile, Italy) connected to a counter for the recording of light-beam interrupts. Before the experiment, the mice were intraperitoneally pretreated with **MBA-159** or vehicle and then, they were individually placed in the activity cages in a sound-attenuated room. The animals' movements (*i.e.*, the number of light-beam crossings) were counted during the next 30 min of the test. Before the experiment, the mice were habituated to activity cages for 15 min [44].

*4.7.3.5. Data analysis.* For the analysis of data obtained in the *in vivo* tests GraphPad Prism software (v. 9.0, CA, USA) was used. Numerical results from the tests are expressed as the mean ± standard error of the mean (SEM). Repeated measures analysis of variance (ANOVA), one-way ANOVA followed by Dunnett's *post hoc* test and Student's *t*-test were used for the statistical analysis of the results. $P < 0.05$ was considered significant.

### *4.8. Treatment with Contilisant and MBA-159 rescued cognitive decline in SAMP8 mice*

#### *4.8.1. Material and methods. Animals*

6-month-old male SAMP8 mice (n = 24) were used to perform cognitive and molecular experiments. Animals had free access to food and water and were maintained under standard temperature conditions (22 ± 2 °C), controlled humidity, and a 12-h light/dark cycle (300 lx/0 lx). Animals were randomized into SAMP8 control (n = 8), SAMP8 **Contilisant** (n = 8), and SAMP8 **MBA-159** (n = 8). The experimental groups received either a daily dose of vehicle (1 % DMSO) (Sigma-Aldrich, Steinheim, Germany, #D4540) with 20 % w/v 2-hydroxypropyl-β-cyclodextrin(Atomole Scientific Co. Ltd., Wuhan, Hubei, China, #AT-20762) or a dose of 10 mg/kg per day of **Contilisant** or **MBA-159** dissolved in vehicle, *via* oral gavage during the treatment period. After 4 weeks of treatment, behavioural cognitive tests were performed. During this period and until sacrifice, the mice received **Contilisant**, **MBA-159** or vehicle.

#### *4.8.2. Behavioural task*

*4.8.2.1. Object location test (OLT).* The OLT was performed to investigate the spatial memory of mice when exposed to a new location of an already-known object. This test is based on the spontaneous tendency of mice to spend more time exploring a novel object than a known object and to recognize when an object has been misplaced. The test was performed in a wooden box (50 × 50 × 25 cm), with three white walls and the last black. The animals were habituated to the empty outdoor area on the first day for 10 min. On the second day, two identical objects were placed in front of the black wall, equidistant from each other and from the wall. The objects were 10 cm high. The animals were brought into the open field arena and allowed to explore the objects and the surroundings for 10 min. The animals were then returned to their home cages, and the OLT apparatus was cleaned with 70 % ethanol. On the third day, an object was relocated in front of the opposite white wall to assess the spatial performance of the mice. Trials were recorded with a camera placed above the open field area, and the total exploration time was determined by counting the time (in seconds) spent sniffing the object at the new location (TN) and the object at the old location (TO). The discrimination index (DI), which is defined as (TN − TO)/(TN + TO), was calculated to assess cognitive performance.

*4.8.2.2. Molecular experiment. RNA extraction and gene expression determination.* RNA was extracted from hippocampal samples using the TRItidy G™ reagent (PannReac AppliChem, #A4051, 0.200) according to the manufacturer's protocol. The purity and quality of the isolated RNA were determinate using the NanoDrop™ ND-1000 device (Thermo Fisher Scientific, Waltham, MA, USA). Only RNA samples with 260/280 ratios between 1.80 and 2.00 were selected for further analysis. Complementary DNA (cDNA) synthesis was carried out using the High-Capacity cDNA Reverse Transcription Kit (Applied Biosystems, #4368813). Quantification of mRNA expression for the selected genes (listed in Table S3, Supporting Information) was performed using SYBR® Green real-time PCR (Applied Biosystems, #K0253) on a StepOnePlus™ Detection System instrument (Applied Biosystems, #4376600). The comparative cycle threshold (ΔΔCt) method was used for data analysis, with β-actin as the housekeeping gene for normalization. Each sample was analysed in duplicate, and the results were expressed as the relative fold change in transcript levels across different experimental groups.

*4.8.2.3. Statistical analysis.* Data was analysed using GraphPad Prism Version 10 (GraphPad Software, San Diego, CA, USA). Results were presented as the mean ± standard error of the mean (SEM). Behavioural tasks included data from 8 individuals, while molecular analyses used 4–6 samples. Group means were compared using one-way ANOVA followed by Tukey's *post hoc* test. For comparisons between two groups, an independent two-tailed Student's *t*-test was applied. Statistical significance was considered when p values were $< 0.05$. Furthermore, statistical outliers were identified and excluded from the analysis using Grubbs' test.

## CRediT authorship contribution statement

**Inaya Nsiona-Defise:** Investigation. **Anna Więckowska:** Supervision. **Aina Bellver-Sanchis:** Investigation. **Paula Zaręba:** Investigation. **Carlos Torrado-Salmerón:** Investigation. **Natalia Szałaj:** Investigation. **Guillermo Torrado Durán:** Investigation. **Christian Griñán-Ferré:** Supervision, Investigation. **Stanislav Gobec:** Supervision. **Francisco López-Muñoz:** Supervision. **Damijan Knez:** Investigation. **Mercè Pallàs:** Supervision. **Ewelina Honkisz-Orzechowska:** Investigation. **Marta Ribalta-Vilella:** Investigation. **Paweł Żmudzki:** Investigation. **Daniel Diez-Iriepa:** Investigation. **Víctor Guarnizo-Herrero:** Investigation. **Aleksandra Manik:** Investigation. **Isabel Iriepa:** Supervision, Investigation. **Borja Martínez-Alonso:** Investigation. **Óscar M. Bautista-Aguilera:** Investigation. **José Marco-Contelles:** Writing – review & editing, Supervision. **Kinga Sałat:** Supervision, Investigation.

## Declaration of Competing Interest

The authors declare no competing financial interest.

## Acknowledgments

II thanks AEI (Government of Spain; Grant PID2019–105813RB-C22). JMC thanks AEI (Government of Spain; Grant PID2019–105813RB-C21) and UCJC [Grant: "In vivo analysis of new analogues of Contilisant (MITOPI) (2022)"] for support. This study was also supported by the Ministerio de Economía, Industria y Competitividad (Agencia Estatal de Investigación, AEI; to CGF, and MP) and Fondo Europeo de Desarrollo Regional (MINECO-FEDER) (PID2022–139016OA-I00, PDC2022–133441-I00, to CGF, and MP), Generalitat de Catalunya (2021 SGR 00357; to CGF and MP). This study was co-financed by Secretaria d'Universitats i Recerca del Departament d'Empresa i Coneixement de la Generalitat de Catalunya 2022 (Producte 0092; Llavor 005 and 007; to CGF). The Government of Catalonia (2021 SGR 00357 to C.G.-F and M.P.). II and OMBA thank Laura Contreras and Cristina García for their collaboration. II and OMBA thank subsidies for the implementation of the research program within the framework of the recovery, transformation and resilience plan – financed by the European Union – Next Generation EU. CAM. K.S. and E.H.-O. thank JUMC for support (Grant N42/DBS/000290 and N42/DBS/000332). ADMET studies were financed by the National Science Centre Poland (Grant No. 2019/34/E/NZ7/00090). The ADMET research/study were carried out with the use of research infrastructure co-financed by the Smart Growth Operational Programme POIR 4.2 project no. POIR.04.02.00–00-D023/20. The financial support from the Slovenian Research and Innovation Agency (Research Core Funding grant P1–0208) is gratefully acknowledged. This research was supported by the Ministry of Education, Science, and Sport (MIZŠ) and the European Regional Development Fund OP20.05187 RI-SI-EATRIS. BMA, VGH, CTS and GTD, thanks UAH CEA and CEMAETA CAI for the *in vivo* pharmacokinetics studies which were carried out with the use of their research infrastructure.

*Supporting information*

The document contains IR, NMR and MS spectra of **MBA-159**, including the IR, NMR and MS for all the intermediates and final target. Molecular modelling and ADME of **MBA-159**.

## Appendix A. Supporting information

Supplementary data associated with this article can be found in the online version at doi:10.1016/j.biopha.2025.118603.

## Data availability

Data will be made available on request.

## References

[1] J. Doroszkiewicz, M. Groblewska, B. Mroczko, Molecular biomarkers and their implications for the early diagnosis of selected neurodegenerative diseases, Int. J. Mol. Sci. 23 (2022) 4610.
[2] M.J. Millan, Y. Agid, M. Brüne, E.T. Bullmore, C.S. Carter, N. Clayton, R. Connor, S. Davis, B. Deakin, R.J. DeRubeis, B. Dubois, M.A. Geyer, G.M. Goodwin, P. Gorwood, T.M. Jay, M. Joëls, I.M. Mansuy, A. Meyer-Lindenberg, D. Murphy, E. Rolls, B. Saletu, M. Spedding, J. Sweeney, M. Whittington, L.J. Young, Cognitive dysfunction in psychiatric disorders: characteristics, causes and the quest for improved therapy, Nat. Rev. Drug Discov. 11 (2012) 141–168.
[3] Alzheimer's Association. Alzheimer's Dement. 17 (2021) 327.
[4] E. Ausó, V. Violeta Gómez-Vicente, G. Esquiva, Biomarkers for Alzheimer's disease early diagnosis, J. Pers. Med 10 (2020) 114.
[5] G. Kim, O. Gautier, E. Tassoni-Tsuchida, X.R. Ma, A.D. Gitler, ALS genetics: gains, losses, and implications for future therapies, Neuron 108 (2020) 822–842.
[6] M.T. Herrero, M. Morelli, M. Multiple mechanisms of neurodegeneration and progression, Prog. Neurobiol. 155 (2017) 1.
[7] F. Fan, H. Liu, X. Shi, Y. Ai, Q. Liu, Y. Cheng, The efficacy and safety of alzheimer's disease therapies: an updated umbrella review, J. Alzheimers Dis. 85 (2022) 1195–1204.
[8] A. Haake, K. Nguyen, L. Friedman, B. Chakkamparambil, G.T. Grossberg, An update on the utility and safety of cholinesterase inhibitors for the treatment of alzheimer's disease, Expert Opin. Drug Saf. 19 (2020) 147–157.
[9] C.H. van Dyck, C.J. Swanson, P. Aisen, R.J. Bateman, C. Chen, M. Gee, M. Kanekiyo, D. Li, L. Reyderman, S. Cohen, L. Froelich, S. Katayama, M. Sabbagh, B. Vellas, D. Watson, S. Dhadda, M. Irizarry, L.D. Kramer, T. Iwatsubo, Lecanemab in early alzheimer's disease, N. Engl. J. Med. 388 (2023) 9–21.
[10] C.J. Suckling, The allure of targets for novel drugs, RSC Med. Chem. 15 (2024) 472–484.
[11] M.J. Oset-Gasque, J. Marco-contelles, alzheimer's disease, the "one-molecule, one-target" paradigm, and the multitarget directed ligand approach, ACS Chem. Neurosci. 9 (2018) 401–403.
[12] O.M. Bautista-Aguilera, J. Budni, F. Mina, E.B. Medeiros, W. Deuther-Conrad, J. M. Entrena, I. Moraleda, I. Iriepa, F. López-Muñoz, J. Marco-Contelles, Contilisant, a tetratarget small molecule for alzheimer's disease therapy combining cholinesterase, monoamine oxidase inhibition, and H3R antagonism with S1R agonism profile, J. Med. Chem. 61 (2018) 6937–6943.
[13] O.M. Bautista-Aguilera, S. Hagenow, A. Palomino-Antolín, V. Farré-Alins, L. Ismaili, P.-L. Joffrin, M.L. Jimeno, O. Soukup, J. Janockova, L. Kalinowsky, E. Proschak, I. Iriepa, I. Moraleda, J.S. Schwed, A. Romero-Martínez, F. López-Muñoz, M. Chioua, J. Egea, R.R. Ramsay, J. Marco-Contelles, H. Shark, Multitarget-directed ligands combining cholinesterase and monoamine oxidase

inhibition with histamine H3R antagonism for neurodegenerative diseases, Angew. Chem. Int. Ed. Engl. 56 (2017) 12765.
[14] J. Romero, R. Martínez-Murillo, M.C. Carreiras, L. Ismaili, ASS234, as a new multi-target directed propargylamine for alzheimer's disease therapy, Front. Neurosci. 10 (2016) 294.
[15] R.R. Ramsay, A. Albreht, Kinetics, mechanism, and inhibition of monoamine oxidase, J. Neural Transm. 125 (2018) 1659–1683.
[16] M. Toledano-Pinedo, A. Porro-Pérez, L. Schäker-Hübner, et al., Contilisant+ Tubastatin a hybrids: polyfunctionalized indole derivatives as new active HDAC inhibitor-based multitarget small molecules with *in vitro* and *in vivo* activity in neurodegenerative diseases, J. Med. Chem. 67 (2024) 16533–16555.
[17] B. Shaker, S. Ahmad, J. Lee, C. Jung, D. Na, In silico methods and tools for drug discovery, Comput. Biol. Med. 137 (2021) 104851.
[18] L. Basile, Virtual screening in the search of new and potent anti-Alzheimer agents, Neuromethods 132 (2018) 107–137.
[19] O. Trott, A.J. Olson, J. A, AutoDock vina: improving the speed and accuracy of docking with a new scoring function, efficient optimization, and multithreading, J. Comput. Chem. 31 (2010) 455–461.
[20] H.O. Gulcan, A. Mavideniz, M.F. Sahin, I.E. Orhan, Benzimidazole-derived compounds designed for different targets of Alzheimer's disease, Curr. Med. Chem. 26 (2019) 3261–3278.
[21] C.A. Lipinski, F. Lombardo, B.W. Dominy, P.J. Feeney, Experimental and computational approaches to estimate solubility and permeability in drug discovery and development settings, Adv. Drug Deliv. Rev. 46 (2001) 3–26.
[22] E.M. Duffy, W.L. Jorgensen, Prediction of properties from simulations: free energies of solvation in hexadecane, octanol, and water, J. Am. Chem. Soc. 122 (2000) 2878–2888.
[23] W.L. Jorgensen, E.M. Duffy, Prediction of drug solubility from Monte Carlo simulations, Bioorg. Med. Chem. Lett. 10 (2000) 1155–1158.
[24] J.F. Wilshire, Intramolecular hydrogen bonding in some ortho-substituted N-methyl-, N-benzyl and N-aryl-4-nitroanilines: a proton magnetic resonance study, Aust. J. Chem. 35 (1982) 2497–2504.
[25] A. Muth, V. Subramanian, E. Beaumont, M. Nagar, P. Kerry, P. McEwan, H. Srinath, K. Clancy, S. Parelkar, P.R. Thompson, R. P, Development of a selective inhibitor of protein arginine deiminase 2, J. Med. Chem. 60 (2017) 3198–3211.
[26] J.J. Newsome, M.A. Colucci, M. Hassani, H.D. Beall, C.J. Moody, Benzimidazole- and benzothiazole-quinones: excellent substrates for NAD(P)H:quinone oxidoreductase, Org. Biomol. Chem. 5 (2007) 3665–3673.
[27] H.-B. Woo, Y.W. Eom, K.-S. Park, J. Ham, C.M. Ahn, S. Lee, Synthesis of substituted benzimidazolyl curcumin mimics and their anticancer activity, Bioorg. Med. Chem. Lett. 22 (2012) 933–936.
[28] I.O. Imosemi, S.E. Owumi, U.O. Arunsi, Biochemical and histological alterations of doxorubicin-induced neurotoxicity in rats: protective role of luteolin, J. Biochem. Mol. Toxicol. 36 (2022) e22962.
[29] N. Okudan, M. Belviranlı, T. Sezer, Potential protective effect of coenzyme Q10 on doxorubicin-induced neurotoxicity and behavioral disturbances in rats, Neurochem. Res. 47 (2022) 1280–1289.
[30] D. Knez, D. Diez-Iriepa, M. Chioua, et al., 8-Hydroxyquinolylnitrones as multifunctional ligands for the therapy of neurodegenerative diseases, Acta Pharm. Sin. B 13 (2023) 2152–2175.
[31] M. Hebda, M. Bajda, A. Wieckowska, N. Szalaj, A. Pasieka, D. Panek, J. Godyn, T. Wichur, D. Knez, S. Gobec, B. Malawska, Synthesis, molecular modelling and biological evaluation of novel heterodimeric, multiple ligands targeting cholinesterases and amyloid beta, Molecules 21 (2016) 410.
[32] A. Więckowska, N. Szałaj, L. Góral, A. Bucki, G. Latacz, K. Kiec-Kononowicz, O. M. Bautista-Aguilera, A. Romero, E. Ramos, J. Egea, V. Faré, A. González-Rodríguez, F. Lopéz-Muñoz, M. Chioua, J. Marco-Contelles, In vitro and in silico ADME-tox profiling and safety significance of multifunctional monoamine oxidase inhibitors targeting neurodegenerative diseases, ACS Chem. Neurosci. 11 (2020) 3793–3801.
[33] A. Elz, N. Trevaskis, C. Porter, J. Bowen, C. Prestodge, Smart design approaches for orally administered lipophilic prodrugs to promote lymphatic transport, J. Control. Release 341 (2022) 676–701.
[34] K. Soulele, V. Karalis, V, Development of a joint population pharmacokinetic model of ezetimibe and its conjugated metabolite, Eur. J. Pharm. Sci. 128 (2019) 18–26.
[35] I. Klinkenberg, A. Blokland, The validity of scopolamine as a pharmacological model for cognitive impairment: a review of animal behavioral studies, Neurosci. Biobehav Rev. 34 (2010) 1307–1350.
[36] U. Košak, B. Brus, D. Knez, S. Žakelj, J. Trontelj, A. Pišlar, R. Šink, M. Jukič, M. Živin, A. Podkowa, F. Nachon, X. Brazzolotto, J. Stojan, J. Kos, N. Coquelle, K. Sałat, J.P. Colletier, S. Gobec, The magic of crystal structure-based inhibitor optimization: development of a butyrylcholinesterase inhibitor with picomolar affinity and in vivo activity, J. Med. Chem. 61 (2018) 119–139.
[37] S.J. Webster, A.D. Bachstetter, P.T. Nelson, F.A. Schmitt, L.J. Van Eldik, Using Mice to Model Alzheimer's Dementia: an Overview of the Clinical Disease and the Preclinical Behavioral Changes in 10 Mouse Models. Front. Genet. 5 (2014I 88.
[38] M. Antunes, G. Biala, The novel object recognition memory: neurobiology, test procedure, and its modifications, Cogn. Process 13 (2012) 93–110.
[39] S.J. Cohen, R.W. Stackman, Jr, Assessing rodent hippocampal involvement in the novel object recognition task. A review, Behav. Brain Res. 285 (2015) 105–117.
[40] K. Sałat, A. Podkowa, S. Mogilski, P. Zaręba, K. Kulig, R. Sałat, N. Malikowska, B. Filipek, The effect of GABA transporter 1 (GAT1) inhibitor, tiagabine, on scopolamine-induced memory impairments in mice, Pharmacol. Rep. 67 (2015) 1155–1162.
[41] A. Ennaceur, J. Delacour, A new one-trial test for neurobiological studies of memory in rats. 1: behavioral data, Behav. Brain Res. 31 (1988) 47–59.
[42] L.M. Lueptow, Novel object recognition test for the investigation of learning and memory in mice, J. Vis. Exp. (2017) 55718.
[43] K. Sałat, K. Gawlik, J. Witalis, D. Pawlica-Gosiewska, B. Filipek, B. Solnica, K. Więckowski, B. Malawska, Evaluation of antinociceptive and antioxidant properties of 3-[4-(3-trifluoromethyl-phenyl)-piperazin-1-yl]-dihydrofuran-2-one in mice, Naunyn Schmiede Arch. Pharmacol. 386 (2013) 493–505.
[44] K. Sałat, A. Podkowa, P. Kowalczyk, K. Kulig, A. Dziubina, B. Filipek, T. Librowski, Anticonvulsant active inhibitor of GABA transporter subtype 1, tiagabine, with activity in mouse models of anxiety, pain and depression, Pharmacol. Rep. 67 (2015) 465–472.
[45] A. Silva, M.C. Martínez, Spatial memory deficits in Alzheimer's disease and their connection to cognitive maps' formation by place cells and grid cells, Front Behav. Neurosci. 16 (2023) 1082158.
[46] J.W. Kinney, S.M. Bemiller, A.S. Murtishaw, A.M. Leisgang, A.M. Salazar, B. T. Lamb, Inflammation as a central mechanism in alzheimer's disease, Alzheimers Dement 4 (2018) 575–590.
[47] N. Faydali, T. O, Arpaci benzimidazole and benzoxazole derivatives against alzheimer's disease, Chem. Biodivers. 21 (2024) e202400123.
[48] A.A. Ibrahim, E.G. Said, A.M. AboulMagd, N.H. Amin, H.M. Abdel-Rahman, Novel benzimidazole hybrids: design, synthesis, mechanistic studies, antifungal potential and molecular dynamics, RSC Med. Chem. 16 (2025) 3291–3311.
[49] B. Liu, J. Liu, J.S. Shi, SAMP8 mice as a model of age-related cognition decline with underlying mechanisms in Alzheimer's disease, J. Alzheimers Dis. 75 (2020) 385–395.
[50] M.Z. Zhong, T. Peng, M.L. Duarte, M. Wang, D. Cai, Updates on mouse models of alzheimer's disease, Mol. Neurodegener. 19 (2024) 23.
[51] P. Verwaerde, O. Défert, AZP2006 (Ezeprogind®): a promising new drug candidate in the battle against neurodegenerative diseases, Chem. Med. Chem. 20 (2025) e202400891.
[52] P. Spatz, T. Zimmermann, S. Steinmüller, J. Hofmann, T. Maurice, M. Decker, Novel benzimidazole-based pseudo-irreversible butyrylcholinesterase inhibitors with neuroprotective activity in an alzheimer's disease mouse model, RSC Med. Chem. 13 (2022) 944.
[53] B. Brooks, R. Bruccoleri, B. Olafson, D. States, S. Swaminathan, M. Karplus, CHARMM: a program for macromolecular energy, minimization, and dynamics calculations, J. Comput. Chem. 4 (1983) 187–217.